



**HAL**  
open science

## **A 2000-year sediment record reveals rapidly changing sedimentation and land use since the 1960s in the Upper Mara-Serengeti Ecosystem**

Christopher Dutton, Amanda Subalusky, Troy Hill, Julie Aleman, Emma Rosi, Kennedy Onyango, Kanuni Kanuni, Jenny Cousins, A. Carla Staver, David Post

### ► To cite this version:

Christopher Dutton, Amanda Subalusky, Troy Hill, Julie Aleman, Emma Rosi, et al.. A 2000-year sediment record reveals rapidly changing sedimentation and land use since the 1960s in the Upper Mara-Serengeti Ecosystem. *Science of the Total Environment*, 2019, 664, pp.148-160. 10.1016/j.scitotenv.2019.01.421 . hal-04471384

**HAL Id: hal-04471384**

**<https://hal.science/hal-04471384>**

Submitted on 23 Feb 2024

**HAL** is a multi-disciplinary open access archive for the deposit and dissemination of scientific research documents, whether they are published or not. The documents may come from teaching and research institutions in France or abroad, or from public or private research centers.

L'archive ouverte pluridisciplinaire **HAL**, est destinée au dépôt et à la diffusion de documents scientifiques de niveau recherche, publiés ou non, émanant des établissements d'enseignement et de recherche français ou étrangers, des laboratoires publics ou privés.

1 **Title**

2 A 2000-year sediment record reveals rapidly changing sedimentation and land use since the  
3 1960s in the Upper Mara-Serengeti Ecosystem

4 **Authors**

5 Christopher L. Dutton<sup>1\*</sup>, Amanda L. Subalusky<sup>2</sup>, Troy D. Hill<sup>3</sup>, Julie C. Aleman<sup>1</sup>, Emma  
6 J. Rosi<sup>2</sup>, Kennedy B. Onyango<sup>4</sup>, Kanuni Kanuni<sup>5</sup>, Jenny A. Cousins<sup>6</sup>, A. Carla Staver<sup>1</sup>  
7 and David M. Post<sup>1</sup>

8 **Affiliations**

9 <sup>1</sup>Yale University, Department of Ecology and Evolutionary Biology, 165 Prospect St,  
10 New Haven, CT, 06511, USA

11 <sup>2</sup>Cary Institute of Ecosystem Studies, 2801 Sharon Turnpike, Millbrook, NY, 12545,  
12 USA

13 <sup>3</sup>South Florida Natural Resources Center, National Park Service, 950 N. Krome Avenue,  
14 Homestead, FL, 33030, USA

15 <sup>4</sup>WWF-Kenya, P.O. Box 62440-0020, Nairobi, Kenya

16 <sup>5</sup>WWF-Tanzania, Plot No. 350, Regent Estate Mikochei, Dar es Salaam, Tanzania

17 <sup>6</sup>WWF-UK, The Living Planet Centre, Rufford House, Brewery Rd, Woking GU21 4LL,  
18 UK

19 \*Corresponding author: Christopher L. Dutton; Yale University, Department of Ecology  
20 and Evolutionary Biology, 165 Prospect St., New Haven, CT 06511; Phone: +1-646-403-  
21 4661; Email: [cldutton@gmail.com](mailto:cldutton@gmail.com)

## 1 **1.0 Introduction**

2 Sustainable development in Africa relies upon using natural resources to promote socioeconomic  
3 development while simultaneously protecting the ecosystem services relied upon by a large  
4 proportion of the population (McClain, 2013). Water has been identified as playing a central role  
5 in both areas (UN-Water, 2003). Water resource planning can increase human access to  
6 improved domestic water sources and improved sanitation, ensure food security through irrigated  
7 agriculture, and contribute to energy security via hydropower, while also conserving and  
8 restoring biodiversity and ecosystem services (McClain, 2013; Sharma et al., 1996; Vörösmarty  
9 et al., 2000). However, water resources are often negatively impacted by land use change  
10 associated with development patterns (Foley et al., 2005). Understanding the impacts of land use  
11 change on river basins and how they relate to historical dynamics is critically important to  
12 making informed decisions about sustainable development and to interpreting present-day  
13 patterns in quantity and quality of water resources (Kundzewicz, 1997; McClain, 2013).

14 The Mara River basin in East Africa is a trans-boundary river basin that highlights many of the  
15 development and conservation challenges in the region. The Mara River flows from its  
16 headwaters in the Mau Forest of Kenya through the northern portion of the Serengeti-Mara  
17 Ecosystem and into Lake Victoria in Tanzania, where it forms part of the headwaters of the Nile  
18 River basin. It is a river basin of international conservation significance, as it is the only  
19 perennial water source in the Serengeti-Mara Ecosystem, and it sustains the largest remaining  
20 overland migration of 1.4 million wildebeest that cross into this basin from the southern  
21 Serengeti during the dry season (Holdo et al., 2009). The Mara River basin also supports an  
22 estimated 1.1 million people, with over 60% of the human population directly reliant upon the

23 river for their domestic water needs (Hoffman, 2007; LVBC and WWF-ESARPO, 2010). The  
24 basin has experienced considerable development in the past few decades, including a 27%  
25 reduction in rangelands, a 32% reduction in forest cover, and a 203% increase in agriculture  
26 between 1973-2003 (Mati et al., 2008).

27 Patterns of increasing development in the Mara River basin are similar to trends throughout East  
28 Africa. Human populations have risen steadily in Kenya and Tanzania since the 1950s (FAO,  
29 2018). Domestic animal populations have also increased since the eradication of rinderpest in the  
30 1960s (Raikes, 1981; Talbot and Talbot, 1963). Some wildlife populations also increased after  
31 rinderpest eradication, while multiple others began declining in the 1970s, partially due to land  
32 use changes and further increases in domestic animal populations (Ogutu et al., 2011; Ogutu et  
33 al., 2016). In the Mara River basin, these land use and land cover changes have likely altered the  
34 hydrology and water quality in the Mara River, leading to increased peak flows, increased  
35 erosion rates, and increased suspended sediments and nutrients in the river (Dutton et al., 2018;  
36 LVBC and WWF-ESARPO, 2010; Mango et al., 2011; Mati et al., 2008; McClain et al., 2014).

37 Increasing suspended sediment loads are a major concern in the Mara River basin; sediment  
38 loads are associated with increases in contaminant loads, and have direct potential consequences  
39 for domestic water users (Hoffman, 2007; LVBC and WWF-ESARPO, 2010). There is also  
40 widespread concern about anthropogenic contaminants in the river due to nutrient runoff from  
41 agricultural fields, human waste from urban settlements and tourism establishments, and mercury  
42 from artisanal gold mining in the basin, among other factors. Mercury contamination is a  
43 particular concern in the lower portion of the Mara River basin, because widespread artisanal  
44 gold mining commonly uses mercury in one of the processing steps (Saldarriaga-Isaza et al.,  
45 2015).

46 Changing populations of wildlife and domestic animals in the Mara River basin may also impact  
47 the long-term sediment and nutrient dynamics in the river. After the eradication of rinderpest, the  
48 Serengeti blue wildebeest (*Connochaetes taurinus*) herd grew from <200,000 to approximately  
49 1.4 million by the late 1970's (Hopcraft et al., 2013), and they contribute 1,100 tons of carcass  
50 biomass per year to the river through mass drownings (Subalusky et al., 2017). The Mara River  
51 also supports a large population of hippopotami (*Hippopotamus amphibius*, hippos), which has  
52 grown by 1500% from the 1950s to over 4,000 individuals (Kanga et al., 2011), and they  
53 contribute 13,200 tons of biomass as feces and urine per year to the river (Subalusky et al.,  
54 2015). As wildebeest and hippo populations have recovered in the Mara, human and livestock  
55 populations also have increased (Ogutu et al., 2016).

56 Here, we have used sediment cores from the Mara Wetland (near its outlet into Lake Victoria) to  
57 evaluate how sedimentation rates and sources have changed historically, through a period  
58 marked by major changes in human and livestock population densities, land use, and disease  
59 epidemics (rinderpest). To do this, we evaluated sediment sources, nitrogen and carbon isotope  
60 signatures, and mercury along a transect of age-calibrated sediment cores in the Mara Wetland,  
61 from the upstream reaches to Lake Victoria. We hypothesized that sediment deposition has  
62 increased overall as human and livestock populations increased through time in the river basin.  
63 Furthermore, we hypothesized that sediment deposition would also increase as a result of land  
64 use change, including deforestation in the Upper Mara sub-catchment and increased livestock  
65 populations in the grazing lands of the Talek, Middle Mara, and Lower Mara sub-catchments,  
66 resulting in changes in sediment provenance in cores. We also hypothesized that both mercury  
67 and nutrient concentrations in the wetland would increase, and that carbon and nitrogen stable  
68 isotope ratios would shift over time to reflect changes from natural to anthropogenic sources.

## 69 **2.0 Materials and Methods**

### 70 *2.1 Study Site*

71 The Mara River is a trans-boundary river shared between Kenya and Tanzania (Fig. 1), and one  
72 of the more pristine basins within the greater Nile Basin of Africa (Mati et al., 2008). The Mara  
73 River basin is approximately 13,500 km<sup>2</sup> and ranges in elevation from 2900 m in the headwaters  
74 to 1130 m at the mouth in Lake Victoria. The Mau Forest Complex forms the headwaters of the  
75 basin and has undergone major changes since the 1970s due to legal and illegal settlements and  
76 deforestation (Olang and Kundu, 2011). The basin also hosts two conservation areas of  
77 international significance: the Maasai Mara National Reserve in Kenya and the Serengeti  
78 National Park in Tanzania.

79 We delineated the Mara River basin into four major sub-catchment areas (Upper Mara, Middle  
80 Mara, Lower Mara, and Talek) based upon drainage patterns from the 15m ASTER Global DEM  
81 dataset, Version 2. The Upper Mara (2450 km<sup>2</sup>, 18% of the basin) accounts for everything  
82 upstream of the Emarti Bridge, including the two main tributaries that form the Mara, the  
83 Nyangores and Amala rivers. This sub-catchment has small-scale settlements, small-scale  
84 agriculture and forested regions that are remnants of the largest indigenous montane forest in  
85 East Africa. The Middle Mara (3010 km<sup>2</sup>, 22% of the basin) includes the main Mara River  
86 channel from the Emarti Bridge to the Purungat (New Mara) Bridge, which is on the border  
87 between Kenya and Tanzania. This sub-catchment primarily consists of wildlife conservancies,  
88 including portions of the Maasai Mara National Reserve, grazing land for domestic livestock  
89 (cattle, goats, and sheep), and tourism facilities. The Lower Mara (5380 km<sup>2</sup>, 40% of the basin)  
90 includes everything downstream of the Purungat Bridge, as well as drainage from land in Kenya

91 near the Lamai Wedge on the west and the Sand River catchment on the east. This region  
92 includes portions of both the conservation areas of the Maasai Mara and Serengeti, and  
93 agricultural areas in Tanzania. The Talek region (2660 km<sup>2</sup>, 20% of the basin) includes the entire  
94 catchment of the Talek River, which is a seasonal and flashy tributary draining semi-arid wildlife  
95 conservancies and grazing lands for domestic livestock. The Upper Mara receives approximately  
96 1400mm per year of rainfall, the Middle and Lower Mara receive approximately 1100mm per  
97 year, and Talek receives approximately 600mm per year (Mati et al., 2008; Mduma et al., 1999).

98 The Mara River flows into Lake Victoria after flowing through the Mara Wetland (also known as  
99 the Masirori swamp) near Musoma, Tanzania (Kassenga, 1997). The Mara Wetland is  
100 approximately 45 km long and up to 14 km wide. Some research suggests the Mara Wetland has  
101 expanded in size by over 300% since the 1970s, which has been hypothesized to be due to  
102 increasing sediment loads and rising lake levels (Mati et al., 2008). The Mara Wetland may play  
103 an important role in buffering the effects of land use changes in the Mara River basin on Lake  
104 Victoria (O'Sullivan et al., 2016). For example, an estimated 75 tons of nitrogen are removed  
105 yearly by the Mara Wetland (Mayo et al., 2013). Lake Victoria is the second largest freshwater  
106 body in the world and of tremendous socioeconomic importance to the region, but its ecosystem  
107 services are at risk due to deteriorating water quality, primarily caused by rivers discharging into  
108 the lake (Odada et al., 2004; Scheren et al., 2000).

109 We delineated the Mara Wetland into four regions (Seasonal Wetland, Upper Wetland, Middle  
110 Wetland, and Lower Wetland) based on evaluations of satellite imagery and field surveys of  
111 changes in vegetation and flow patterns conducted in August, 2015. The Seasonal Wetland  
112 region is the most upstream portion of the Mara Wetland, where the river is still primarily  
113 confined to one incised channel. Small-scale agriculture takes place on the fringes of the

114 Seasonal Wetland and, in some instances, within it. Papyrus and other common wetland plants  
115 primarily begin in the Upper Wetland section and the channel begins to bifurcate multiple times.  
116 Most of the Middle Wetland is not navigable due to dense, floating papyrus mats that impede  
117 travel. The Lower Wetland is deeper (up to 25 meters) and directly tied to the hydrology of Lake  
118 Victoria. The boundaries between these regions are somewhat arbitrary and likely dynamic  
119 depending on recent precipitation. Low-impact artisanal fishing involving nets occurs within all  
120 navigable portions of the wetland.

## 121 *2.2 Sediment Core Collection and Processing*

122 Four sets of cores were taken from the four distinct areas of the Mara Wetland. The Seasonal  
123 Wetland set of cores were taken just downstream of the Seasonal Wetland area within a  
124 constrained channel just prior to a bifurcation in the channel. The Upper Wetland core set was  
125 taken within a shallow lake (approximately 0.5 km<sup>2</sup>) in the middle of the Upper Wetland section.  
126 The Middle Wetland core was taken in the middle portion of the wetland that was cut off from  
127 navigation from the other portions of the wetland. The Lower Wetland core was taken near the  
128 entry point into Lake Victoria (Fig. 1).

129 Sediments were cored from a stable, floating platform built at the site that consisted of several  
130 sheets of wood placed on two inflatable air mattresses. We collected sediment cores in August,  
131 2015, at the sediment-water interface using a Universal Corer (Aquatic Research Instruments,  
132 Hope, Idaho, USA) at four sites in distinct portions of the wetland (Fig. 1). Each Universal core  
133 (UC) included approximately 0.5 to 1 m in depth below the sediment-water interface. At two of  
134 those sites, we also collected deeper cores using a Russian Peat Borer (Aquatic Research  
135 Instruments, Hope, Idaho, USA), each segment of which was 50 cm in depth. These Russian  
136 cores (RCs) were collected at an approximately 1-meter offset from the location of the Universal

137 cores, starting at the deepest point collected with the previous core with a 10 cm vertical overlap  
138 between each 50 cm depth intervals. Russian cores were collected to the maximum depth we  
139 were able to access by manually pushing and retrieving the corer through the wetland sediments.  
140 Universal cores were immediately extruded and sectioned in the field into 1 cm intervals and  
141 sealed in air-tight Ziploc polyethylene bags. Entire Russian cores were sealed in the field with  
142 saran wrap to prevent desiccation and taped into PVC tubes to prevent shrinking or damage  
143 during transport. All samples were shipped wet from Tanzania to Yale University and arrived  
144 within several days.

145 In the lab, we processed the top core sections from all four cores (Seasonal Wetland, Upper  
146 Wetland, Middle Wetland, and Lower Wetland) for  $^{210}\text{Pb}$  dating. We processed additional deeper  
147 cores for radiocarbon dating from the Seasonal Wetland (consisting of UC7, RC9, RC10, RC11,  
148 and RC12) and the Upper Wetland (consisting of UC11, RC21, and RC23). All Russian cores  
149 from those two sites were sectioned into 1 cm intervals. Portions of the 1 cm sections from the  
150 universal cores and Russian cores were then dried at 60° C and re-weighed to obtain bulk mass  
151 density estimates. The dried portions were then gently disaggregated with a mortar and pestle to  
152 obtain a homogenous sample and apportioned to dating, sediment fingerprinting, carbon and  
153 nitrogen isotopic analysis, and mercury analysis.

### 154 *2.3 Dating and Age-Depth Model*

155 We used lead-210 ( $^{210}\text{Pb}$ ; 22.3 yr half-life) to assign ages to sediment deposited during the past  
156 110 years (five half-lives). Geochemical measurements were made on subsamples dried to 60°C.  
157 Dried, ground samples were sealed in 10 mL scintillation vials, and equilibrated for at least 21  
158 days before analysis. This equilibration period allowed supported  $^{210}\text{Pb}$  ( $^{210}\text{Pb}$  produced by in-

159 situ decay of  $^{226}\text{Ra}$ , measured indirectly as  $^{214}\text{Pb}$ ) to be distinguished from unsupported or excess  
160  $^{210}\text{Pb}$  ( $^{210}\text{Pb}_{\text{xs}}$ ). Activities of  $^{210}\text{Pb}$  and  $^{214}\text{Pb}$  were measured by gamma ray spectrometry using a  
161 low-background Ge detector.  $^{210}\text{Pb}$  and  $^{214}\text{Pb}$  activities were measured at energies of 46.5 and  
162 352.7 keV, respectively, and were corrected for detector efficiency and self-absorption (Cutshall  
163 et al., 1983).

164 We also measured  $^{137}\text{Cs}$  in the upper portions of the Seasonal Wetland, Upper Wetland, Middle  
165 Wetland and Lower Wetland cores.  $^{137}\text{Cs}$  was distributed globally during atmospheric nuclear  
166 testing in the 1950s and 1960s and can be used as an independent time marker for the age-depth  
167 model (Ritchie and McHenry, 1990).

168 We created age-depth models using the Plum model for the Bayesian analysis of  $^{210}\text{Pb}$  dating for  
169 the upper portions of the Upper Wetland, Middle Wetland, and Lower Wetland cores (Aquino-  
170 López et al., 2018). We did not create an age-depth model for the Seasonal Wetland core due to  
171 mixing throughout the depth of the core (see results and discussion below). The Plum model is  
172 loosely based on the CRS model, which allows sedimentation rates to vary (Aquino-López et al.,  
173 2018; Oldfield and Appleby, 1984; Robbins, 1978). The Plum model retains two of the basic  
174 assumptions of the CRS model, including (1) that supply of  $^{210}\text{Pb}$  is constant, and (2) that there is  
175 no vertical displacement of radionuclides (i.e., no mixing or post-depositional diagenesis).  
176 However, a continuous inventory of  $^{210}\text{Pb}$  from the entire core is not required and it is not  
177 necessary to achieve background in order to formulate the model.

178 The Plum model is formulated within a robust statistical framework to natively quantify any  
179 uncertainty within the modelled dates (Aquino-López et al., 2018). Plum uses a self-adjusting  
180 Markov Chain Monte Carlo (MCMC) algorithm known as the  $t$ -walk (Christen and Fox, 2010).

181 Use of the  $t$ -walk requires very little customization in setting the default model parameters.  
182 Changes in sedimentation accumulation are calculated through millions of iterations of the  
183 MCMC using the same gamma autoregressive semiparametric age-depth function contained  
184 within *Bacon*, a popular age-depth model for paleoclimate reconstructions (Blaauw and Christen,  
185 2011). Full details of the Plum model formulation can be found in Aquino-López et al. (2018).

186 We used radiocarbon dating to date samples at longer time scales than  $^{210}\text{Pb}$  dating. We dried  
187 samples at  $45^\circ\text{C}$  and then submitted bulk sediments to the Lawrence Livermore National  
188 Laboratories (LLNL, Livermore, California, USA) for radiocarbon dating. Samples appeared  
189 homogeneous with no obvious evidence of macrofossils. All samples were subjected to the  
190 standard pretreatment steps at LLNL, including the acid-base-acid chemical pretreatment, in  
191 order to remove carbonates. Radiocarbon dating was thus performed in the total organic carbon  
192 (TOC) of the bulk sediments, preventing any potential aging effects of the carbonates (Bronk  
193 Ramsey, 2008). Five radiocarbon dates were measured for the Seasonal Wetland core set (UC7,  
194 RC9, RC10, RC11, and RC12) and four radiocarbon dates were measured for the Upper Wetland  
195 core set (UC11, RC21, and RC23) (Fig. S1). The dates were calibrated using the IntCal13 curve  
196 implemented in *Bchron* in R (Parnell, 2016; Reimer et al., 2013).

197 We built a Bayesian age-depth model using *Bchron* in R for the Upper Wetland core (Haslett and  
198 Parnell, 2008; Parnell, 2016). In the age-depth model, we used all of the radiocarbon dates (4  
199 total) and a subset of the  $^{210}\text{Pb}$ -modelled dates (7 total) to prevent the age-depth model from  
200 being unfairly biased towards the  $^{210}\text{Pb}$ -modelled dates (Fig. 4) (Kemp et al., 2013). We used the  
201 standard program settings for creation of the age-depth model (Parnell, 2016).

202 Sediment accretion and mass accumulation rates were calculated from  $^{210}\text{Pb}_{\text{xs}}$  data for the top  
203 sections of the Upper Wetland (UC11), Middle Wetland (UC15), and Lower Wetland (UC1)  
204 cores using the Plum model for the Bayesian analysis of  $^{210}\text{Pb}$  dating (Aquino-López et al.,  
205 2018). Sediment accretion and mass accumulation rates were also calculated for the entire Upper  
206 Wetland core set using the full age-depth model ( $^{210}\text{Pb}_{\text{xs}}$  and radiocarbon dates) created in  
207 *Bchron* (Parnell, 2016). Accretion rates ( $r_i$ ;  $\text{cm} \cdot \text{yr}^{-1}$ ) for each core section,  $i$ , at each depth,  $x$ , at  
208 each time,  $t$ , were calculated as:

$$209 \quad r_i = \frac{x_i - x_{i-1}}{t_i - t_{i-1}} \quad (\text{Eq. 1})$$

210 Accretion rates were then used to calculate mass accumulation rates:

$$211 \quad \text{MAR}_i = r_i \times \rho_i \quad (\text{Eq. 2})$$

212 where  $\text{MAR}_i$  is the mass accumulation rate ( $\text{g} \cdot \text{cm}^{-2} \cdot \text{yr}^{-1}$ ) for a depth interval  $i$ , and  $\rho_i$  is the  
213 corresponding bulk density ( $\text{g sediment} \cdot \text{cm}^{-3}$ ).

#### 214 *2.4 Sediment Fingerprinting*

215 We used the sediment fingerprinting method developed in Dutton et al. (2013) to trace the source  
216 of sediments from each layer of the Seasonal Wetland and Upper Wetland cores. A brief  
217 description of our methods is described here, and a more detailed description is in  
218 Supplementary Material 1.

219 We collected 39 composite soil samples throughout 7 different major lithology groups of the  
220 Lower Mara region to build a composite sediment fingerprint for that region (Fig. S2). Samples  
221 were dried, gently disaggregated, and sieved to  $< 63 \mu\text{m}$ . Samples were then analyzed for 59

222 elements with a multi-acid total digestion on an ICP-MS by Bureau Veritas Acme Labs  
223 (Vancouver, BC Canada).

224 Source signatures were previously developed for Kenyan sources (Upper Mara, Middle Mara,  
225 and Talek) and for hippos (hippo feces) for a subset of the elements analyzed during this  
226 sampling campaign (Dutton et al., 2013). We built upon those signatures by collecting additional  
227 suspended sediments from the Upper Mara ( $N = 3$ ) and Talek ( $N = 7$ ) from 2012 through 2015.  
228 In total, 28 elements were measured within both campaigns and considered for use as tracers.

229 Source signatures for Upper Mara and Talek were based on suspended sediment samples  
230 collected in the river, and Middle Mara and Lower Mara were based on soil samples from the  
231 different lithologies of those sub-catchments. We minimized potential artifacts of these different  
232 sample types by only analyzing the fine fraction of the soil samples ( $<0.63 \mu\text{m}$ ), which is a  
233 widely accepted approach to reduce potential particle size influence on elemental signatures  
234 (Collins et al., 2017). Additionally, we collected suspended sediment samples during different  
235 flow events and discharges to capture the natural variability occurring within each sub-catchment  
236 (Dutton et al., 2013).

237 We used a simplified tracer screening approach similar to Blake et al. (2018). First, we removed  
238 elemental concentrations from the depositional samples that fell outside the minimum detection  
239 limits or the natural range of the sources. We then used a Kruskal-Wallis  $H$ -test to identify  
240 tracers that showed significant differences between the potential sources (Supplementary  
241 Material 2) (Kruskal and Wallis, 1952; R Core Team, 2018). To characterize the discrimination  
242 ability of the combination of elements, we used a step-wise Discriminant Function Analysis  
243 (DFA) based on the minimization of Wilk's lambda and a jackknifed Discriminant Function  
244 Analysis (jDFA) (Venables and Ripley, 2002; Weihs et al., 2005). Overall success with the

245 leave-one-out classification (jDFA) was 93%. We then used MixSIAR, a Bayesian mixing  
246 model, to estimate the source proportions for each core slice (Moore and Semmens, 2008; Stock  
247 et al., 2018; Stock and Semmens, 2016). We then applied the Bayesian age-depth model  
248 incorporating the modelled  $^{210}\text{Pb}$  and radiocarbon dates to the source proportions for each core  
249 slice to determine sediment source proportions through time.

### 250 *2.5 Mercury*

251 We measured total mercury concentration in sediment layers from universal cores from three  
252 different locations along a transect through the Mara Wetland: Upper Wetland, Middle Wetland  
253 and Lower Wetland (Fig. 1). Samples were dried, ground with a mortar and pestle, and analyzed  
254 on a Direct Mercury Analyzer (DMA80, Milestone, Shelton, CT, USA).

### 255 *2.6 Carbon and Nitrogen Isotopes*

256 The dried and ground sediment samples from the Upper Wetland core set (UC11, RC21, and  
257 RC23) were fumigated in hydrochloric acid vapor for 48 hours to remove inorganic C  
258 (Jaschinski et al., 2008; Ramnarine et al., 2011). We then measured the percent by mass of total  
259 organic carbon and total nitrogen, as well as the stable isotope ratios of carbon (total organic  
260  $\delta^{13}\text{C}$ ) and nitrogen (total  $\delta^{15}\text{N}$ ), on a Costech elemental analyzer (Costech Analytical  
261 Technologies Inc., Valencia, CA, USA). Stable isotope ratios were normalized to air ( $\delta^{15}\text{N}$ ) and  
262 Vienna Pee Dee Belemnite ( $\delta^{13}\text{C}$ ) scales and reported in per mil notation, where  $\delta^{15}\text{N} = [(R_{\text{sample}} -$   
263  $R_{\text{air}})/R_{\text{air}}] \times 10^3$  and  $\delta^{13}\text{C} = [(R_{\text{sample}} - R_{\text{PDB}})/R_{\text{PDB}}] \times 10^3$ .

264 All statistical analyses were computed in R 3.5.1 in RStudio 1.1.453 (R Core Team, 2018;  
265 RStudio Team, 2016). All R code and data for conducting the analyses and preparing the figures

266 are provided in Supplementary Material 2, 3, and the Mendeley Data online data repository  
267 (Dutton et al., 2019).

## 268 **3.0 Results**

### 269 *3.1 Dating and Age-Depth Model*

270 The Seasonal Wetland core showed evidence of mixing throughout the upper portion of the core  
271 with no discernable pattern in the  $^{210}\text{Pb}$  data (Fig. 2). The radiocarbon dating chronology for the  
272 Seasonal Wetland core set (UC7, RC9, RC10, RC11, and RC12) further indicated a strong  
273 mixing of sediments (Table 1). We found  $^{14}\text{C}$  ages alternating between modern and  
274 approximately 300 [yr BP] from 4 tested samples down to at least 159cm below the sediment  
275 surface (Table 1). The bottom of the deepest part of that core set (RC12) was at 189cm below the  
276 sediment surface and it was dated at  $2625 \pm 50$   $^{14}\text{C}$  age [yr BP] (Table 1), indicating that the  
277 mixing zone within that core set stopped somewhere between 159cm and 189cm. Mixing of  
278 sediments within this core was likely due to the geomorphology of this wetland section and the  
279 presence of frequent disturbances in the channel. The river flows through a constrained channel  
280 at this sampling point, and we sampled immediately upstream of a bifurcation in the channel  
281 where we believed sediment would accumulate. However, the data suggest this location was not  
282 a stable depositional zone, so we did not create an age-depth model for this core.

283 Excess  $^{210}\text{Pb}$  activity from the Upper Wetland, Middle Wetland, and Lower Wetland showed a  
284 general decrease in activity through the depth of the core and the potential presence of mixing in  
285 the upper portion of the cores. Bayesian-modelled dates based on the excess  $^{210}\text{Pb}$  activity were  
286 computed for each depth in the Upper Wetland, Middle Wetland and Lower Wetland cores (Figs.  
287 2 and 3). In all three cores, the Plum age-depth model indicated more rapid sediment accretion

288 and accumulation in recent years; however, this pattern was more pronounced in the Upper  
289 Wetland core and declined going downstream to Lake Victoria (Upper Wetland, Middle  
290 Wetland, and Lower Wetland) (Fig. 4). Model confidence was greatest in the Upper Wetland  
291 core (Fig. 3).

292 The use of  $^{210}\text{Pb}$  derived age-depth models requires an independent corroboration to establish  
293 that the model is reasonable (Smith, 2001). We attempted to use  $^{137}\text{Cs}$  as an independent time  
294 marker but detected very low levels of it in all four cores (Fig. S3). The Upper Wetland Core had  
295 a small peak at 29cm that doubled background levels ( $\sim 6 \text{ Bq Kg}^{-1}$ ). We constructed an age-depth  
296 model for the Upper Wetland core using the  $^{210}\text{Pb}$  data and the independent time marker of the  
297  $^{137}\text{Cs}$  peak and the dates after 1960 were very similar. However, accumulation rates and dates  
298 prior to 1960 were non-sensical (indicating an exponential decrease in erosion between the 1950s  
299 and 1960s, see Supplementary Material 2), so we utilized the age-depth model without the use of  
300 the  $^{137}\text{Cs}$  peak. Our inability to utilize  $^{137}\text{Cs}$  in this system may be due to the general low levels  
301 of fallout in the southern hemisphere and because  $^{137}\text{Cs}$  may be non-conservative and mobile in  
302 the anoxic sediments of the Mara Wetland (Benoit and Rozan, 2001; Comans et al., 1989; Davis  
303 et al., 1984; Drexler et al., 2018; Wang et al., 2017). Other studies in equatorial Africa have also  
304 reported low  $^{137}\text{Cs}$  levels that made the radioisotope unreliable as an independent stratigraphic  
305 marker (Nyarko et al., 2016). Because we were unable to use  $^{137}\text{Cs}$  as an independent time  
306 marker, we compared our age-depth models to historical trends of precipitation, the historical  
307 water level of Lake Victoria, and prior watershed erosion modelling to establish that our  $^{210}\text{Pb}$   
308 derived age-depth models are reasonable (see discussion).

309 Elevated  $^{210}\text{Pb}$  concentrations in the Upper Wetland core suggest that  $^{210}\text{Pb}$  has been imported to  
310 this area in excess of expected atmospheric deposition (Turekian et al., 1983). It is likely that

311 land use changes within the basin and variable inputs of rainfall and sedimentation since the  
312 1960s affected the  $^{210}\text{Pb}$  input to the wetland (Baskaran et al., 2014). Although the  
313 concentrations diverge substantially, the modeled sediment accumulation rates are quite similar  
314 overall (Fig. 4), providing some confidence that artifacts are temporally constant or otherwise  
315 insubstantial and accounted for within the confidence intervals of the Plum Bayesian model.

316 The radiocarbon dating chronology for the Upper Wetland core set (UC11, RC21, and RC23)  
317 showed that the core ranged from present to 1839 years BP (Table 1). Results from the Bayesian  
318 age-depth model indicated that sediment deposition was not linear through time, and that  
319 deposition rates were most rapid in recent years (Fig. 5).

### 320 *3.2 Sediment Fingerprinting*

321 We found changing sediment sources over time in the Upper Wetland Core set (UC11, RC21,  
322 and RC23) (Fig. 6). The Upper Mara was responsible for the greatest proportion of sediments  
323 throughout the set of Upper Wetland cores (Fig. 6). Lower Mara and Talek sources make up the  
324 next two largest sources of sediment in the core. The proportion of sediments from Upper Mara  
325 began declining in the late 1700s, with the other sources increasing in proportion. Changes  
326 became most pronounced in the mid-1970s (Fig. 6). The proportion of sediment contributed by  
327 the Upper Mara declined markedly from ~50-60% of the sediments in the wetland to ~40% in  
328 the late 1980s. At the same time, sediment contribution from the Talek portion of the basin  
329 increased from <10% to ~20%. Sediment loads from the Lower Mara have provided  
330 approximately the same proportion of sediments relative to the other sources (~30%).

331 In addition to changes in the source of sediments, the total amount of sediment accumulating in  
332 the wetland from each portion of the basin has continued to increase, particularly since the

333 1960s, coincident with the rise in populations of human and cattle in Kenya and Tanzania (Figs.  
334 7A and 7B). The largest quantity of sediment is provided by the Upper Mara, followed by Lower  
335 Mara and then Talek and Middle Mara.

336 The MixSIAR mixing model confirmed that the core slices in the Seasonal Wetland core (UC7)  
337 are all likely well mixed with one another, with no change in sediment source over the depth of  
338 the core (Fig. S4). Plots of key elements as well as bulk density, nitrogen, carbon, and mercury,  
339 confirm a relatively homogeneous upper core section indicative of a mixed column of sediments  
340 (Figs. S5 and S6). In contrast, plots of key elements from the non-mixed Upper Wetland core  
341 exhibited clear changing patterns throughout the depth of the core in multiple elements (Figs. S7  
342 and S8) which would be indicative of a non-mixed core.

### 343 *3.3 Mercury*

344 Mercury data for the Upper Wetland core had a historic baseline ~20 ppb that began increasing  
345 gradually in the 1700s (Fig. 8A). Concentrations briefly stabilized at ~30 ppb in the 1950s before  
346 increasing in the 1960s to ~50 ppb, which is 2.5 times historic background concentrations. In  
347 1984, concentrations began declining to ~25 ppb, found in the upper region of this core.

348 We also examined patterns in mercury concentration over the last 50-100 years along a transect  
349 through the wetland (Fig. 8B). Mercury concentrations in the Middle Wetland core increased  
350 from 25 to 35 ppb from 1950 to 2000, which is similar to the concentration changes in the Upper  
351 Wetland core. Concentrations have begun to increase again at this site in the last 20 years, rather  
352 than declining as at the Upper Wetland site. The Lower Wetland core shows a different pattern,  
353 with a slight decrease in mercury levels from 1900-1990, followed by a sharp decrease and  
354 recovery of mercury concentrations (Fig. 8B).

### 355 3.4 Carbon and Nitrogen Isotopes

356 The percent C and N in the Upper Wetland began increasing in the early 1900s, peaked from  
357 1960-80, and then declined to levels just below the historic baseline from 1990 to present (Fig.  
358 9A). Interestingly, both the percent C and N, and the C:N ratio (Fig. S9), declined through the  
359 1970's and 80's to modern-day levels.

360 C and N stable isotope ratios follow different patterns over this time period (Fig. 9B). Looking at  
361 a longer historical time period, from 1000-1950 AD,  $\delta^{13}\text{C}$  is relatively constant at -14 to -16‰,  
362 which aligns with the isotopic ratio of C4 savanna grasses in the Mara watershed (Fig. 9B)  
363 (Masese et al., 2015; Masese et al., 2018). From ~1950-70, this value declines to -20‰, which is  
364 closer to the ratio of C3 plants such as trees. The  $\delta^{13}\text{C}$  ratio then increases in 1980-90 to an  
365 intermediate value of -17‰.

366 For  $\delta^{15}\text{N}$  ratios, the historical baseline was relatively stable between 2-4‰ from 1000 to 1960  
367 (Fig. 9B). The  $\delta^{15}\text{N}$  ratio increased gradually from 1960 to 1980, and then increased dramatically  
368 through the 1990's, when it stabilized at elevated values around 6‰ over the past 20 years.

## 369 4. Discussion

370 Multiple lines of evidence suggest ecological conditions in the Mara River basin were fairly  
371 stable over paleoecological time scales (2000-1000 years before present), but there has been a  
372 period of rapid change in the basin over the last 250 years, particularly since the 1960s, likely  
373 due to anthropogenic factors. The earliest changes in the basin began in the mid-1700s, including  
374 increased sediment, mercury, and nutrient loads, and these changes corresponded with the advent  
375 of the Industrial Revolution and the increased presence of colonial settlers in East Africa by the

376 late 1800s (Shillington, 2012). More pronounced changes in the origin and quantity of sediments,  
377 mercury concentrations, and C and N stable isotope ratios began in the 1960s.

378 The highest proportion of suspended sediment has always come from the Upper Mara, which is  
379 to be expected since this region has the highest elevational changes and the highest rainfall  
380 (McClain et al., 2014). However, the proportion of total sediment entering the wetland from the  
381 Upper Mara region has decreased from ~50% to ~40% since the late 1700s, and particularly in  
382 the 1950s and 1960s, even as the quantity of sediment from the Upper Mara has increased (Figs.  
383 6 and 7). Much of this change in proportional load is due to increased quantity and proportion of  
384 sediment from the Talek portion of the basin, which increased from <10% of total sediments in  
385 the 1970s to ~20% in recent years.

386 Contemporary research from 2011 through 2014 measuring high temporal resolution sediment  
387 fluxes found that the combined Middle Mara-Talek sub-catchment contributes twice the  
388 sediment flux as the Upper Mara sub-catchment (Dutton et al., 2018). This study found that the  
389 Middle Mara and Talek sub-catchments contributed an average of 8% and 21% of the sediments  
390 from 2010 through 2015 compared to 33% from the Upper Mara. Although within the same  
391 order of magnitude, the difference between the two methods may reflect the transport and  
392 storage of sediments within the river channel or banks. Sediments mobilized from Talek and  
393 other areas of the basin may take several years to decades to reach the wetland. Previous studies  
394 have shown the floodplains and river channels are important for sediment storage dynamics in  
395 rivers (Wallbrink et al., 1998; Walling et al., 2003). Overall, these data suggest recent land-use  
396 change in the Talek may be causing this portion of the basin to become an increasingly important  
397 source of sediments in the region which have not yet reached the wetland. A delay in the timing  
398 between when sediment is mobilized in the catchment and when it reaches the Mara Wetland

399 would suggest there may be some error in our estimates of the time of land use change in the  
400 basin. However, we expect this time lag to be relatively short, given the alignment of sediment  
401 dynamics in the wetland with known timing of land use change in the basin.

402 Our findings provide support for earlier work using remote sensing showing that the Mara  
403 Wetland has expanded in size since the 1970s due to sediment accumulation in the upper  
404 portions of the wetland (Mati et al., 2008). In all the cores analyzed, the Plum Bayesian age-  
405 depth models indicate more rapid sediment accumulation in recent decades (Fig. 4). As sediment  
406 deposition accelerated, the Plum models suggest the wetland served as a sediment trap, with  
407 higher rates of sediment accumulation occurring in the upstream portions away from Lake  
408 Victoria. Interestingly, the age-depth model indicated that sediment accumulation rose rapidly in  
409 the Lower Wetland after 1996 and fell again just prior to 2009 (Fig. 4). This change likely  
410 coincided with a rapid increase in the water level of Lake Victoria in 1998 and subsequent  
411 decline in water level up to 2007 (Vanderkelen et al., 2018). As Lake Victoria rose, hydrological  
412 connectivity likely increased between the lower and middle portions of the wetland and the  
413 mainstem river upstream, which would have reduced water residence time in the wetland and the  
414 corresponding buffering capacity of wetland vegetation and allowed more sedimentation to reach  
415 further through the wetland towards Lake Victoria (Bavor and Waters, 2008; Kansiime et al.,  
416 2007). A similar, but smaller, peak was also observed in the Middle Wetland between 1998 and  
417 2009 (Fig. 4).

418 Sediment accumulation dynamics in the wetland also likely reflect large-scale precipitation  
419 patterns in the basin. The sediment fingerprinting analysis from the Upper Wetland core  
420 identified an overall increase in sediment accumulation from all sources since the 1960s.  
421 However, there has been an oscillation in sediment accumulation rates from all sources since the

422 late 1970s (Fig. 7B). This pattern may reflect the natural decadal oscillation in rainfall patterns in  
423 concert with increasing rainfall extremes experienced in the Mara since the 1960s (Fig. 10)  
424 (Bartzke et al., 2018). A series of wetter years with extreme floods would be capable of  
425 transporting more sediments than those transported by the succeeding period of drier years with  
426 extreme droughts. The sediment accumulation rates from the age-depth model roughly  
427 corresponded to historical rainfall records, showing decreased sediment accumulation rates in  
428 periods of extreme droughts and higher sediment accumulation rates after periods of higher  
429 annual rainfall (Fig. 10).

430 Further support for our age-depth models and sediment accumulation rates can be found by  
431 comparing our sediment accumulation rates to modelled erosion rates using land use, slope, and  
432 soil characteristics in the basin. Using land cover data from 2003, Defersha et al. (2012) used the  
433 *Erosion 3D* model to calculate the expected amount of erosion in the combined Upper Mara,  
434 Middle Mara and Talek sub-catchments to be  $0.3 \text{ g cm}^{-2} \text{ yr}^{-1}$ . Using the results of our age-depth  
435 model, sediment fingerprinting proportions and calculated sediment accumulation rates, we  
436 found that the amount of erosion in 2003 from the combined Upper Mara, Middle Mara and  
437 Talek sub-catchments was approximately  $0.2 \text{ g cm}^{-2} \text{ yr}^{-1}$  (95% confidence intervals between 0.08  
438 and  $0.35 \text{ g cm}^{-2} \text{ yr}^{-1}$ , Fig. 7). Additionally, the trend of a contemporary increase in sediment  
439 accumulation rate found with our  $^{210}\text{Pb}$  age-depth model is independently supported by an  
440 increase in modelled erosion rates based on satellite-derived land cover changes using the  
441 Revised Universal Soil Loss Equation in the Lower Mara sub-catchment between 1986 and 2013  
442 (Århem and Fredén, 2014), and satellite-derived land cover changes from the Upper Mara,  
443 Middle Mara, and Talek sub-catchments between 1976 and 2014 indicating an increase in  
444 agricultural lands (Mwangi et al., 2018), which historically accounts for the highest rate of

445 erosion in the basin (Defersha et al., 2012). Contemporary high temporal resolution  
446 measurements from 2012 to 2015 of suspended sediment flux from the Upper Mara, Middle  
447 Mara and Talek sub-catchments also indicate the potential for yearly increases, although yearly  
448 trends were not calculated because several months were missing from each hydrological year  
449 (Dutton et al., 2018).

450 Age-depth modelling using  $^{210}\text{Pb}$  in catchments with dynamic sediment regimes can be  
451 challenging (Abril et al., 2018; Kirchner, 2011). Data that violates the age-depth model  
452 assumptions can lead to incorrect dates and spurious sediment accumulation rates (Abril et al.,  
453 2018; Bachmann et al., 2018). The Plum model we use to analyze  $^{210}\text{Pb}$  dating is based on the  
454 CRS model, but does not require that  $^{210}\text{Pb}$  measurements quantify the total inventory of  $^{210}\text{Pb}$   
455 (Aquino-López et al., 2018; Mabit et al., 2014). The non-monotonic decreases in  $^{210}\text{Pb}$  that we  
456 observed in the upper portion of our cores could represent an increase in the sediment  
457 accumulation rate or the presence of mixing (Arias-Ortiz et al., 2018), which can result in an  
458 overestimation of sediment accumulation rates (Arias-Ortiz et al., 2018; Mabit et al., 2014). Our  
459  $^{210}\text{Pb}$  concentrations by depth may not represent the ideal conditions for age-depth modelling, so  
460 we have used both independent corroborations of our estimated sedimentation rate and a  
461 statistical framework that incorporates uncertainty (Aquino-López et al., 2018). Additionally, we  
462 focus our analysis on decadal trends in the upper portions of our cores rather than attempt to  
463 infer high temporal resolution year-to-year changes due to the uncertainty present in our models  
464 (Fig. 3). Our age-depth models and sediment accumulation rates are congruent with  
465 contemporary increases in suspended sediment concentrations, prior watershed erosion  
466 modelling using remote sensing of land use change, historical precipitation regimes, and the  
467 historical water level for Lake Victoria.

468 Mercury concentrations followed a similar pattern as sediment dynamics in the basin. There was  
469 an initial modest increase in mercury concentrations after the late 1700s that was likely caused  
470 by atmospheric deposition reflecting global increases in industrialization (Driscoll et al., 2007).  
471 The more rapid increase in the 1950s and 1960s was likely due to a combination of deforestation  
472 and artisanal mining (Gamby et al., 2015; Telmer and Veiga, 2009), which was also reflected in  
473 the large changes in sediment source and quantity during this time. Mercury binds to organic  
474 material and will remain in forested soils, only becoming mobilized when the soils are disturbed  
475 through deforestation or other land use conversions (Gamby et al., 2015; Schwesig et al., 1999).  
476 Similar increases in mercury concentration were documented in response to loss of native land  
477 cover in the Amazon during the same time period (Roulet et al., 2000). However, the decline in  
478 the 1980s, stabilizing at concentrations only slightly elevated above the historical baseline,  
479 suggests there has been a reduction in mercury loads into the Mara Wetland over the last 20  
480 years (Fig. 8). The recent decrease in mercury concentration could be due to the higher relative  
481 impact of initial loss of native land cover that is now stabilizing, or to conservation initiatives in  
482 the upper basin aimed at decreasing soil erosion and runoff (Gamby et al., 2015). There are no  
483 available data about the historical occurrence or frequency of artisanal gold mining in the Mara  
484 River basin, which impedes our quantifying the proportion of mercury contamination that can be  
485 attributed to this process.

486 All mercury concentrations are below the National Oceanic and Atmospheric Administration's  
487 (NOAA) Effects Range-Low (150 ppb; ERL) concentration, which was associated with adverse  
488 biological effects in 10% of studies reviewed by NOAA, suggesting that current mercury  
489 contamination is unlikely to pose an ecological risk in the Mara Wetland. Our data also suggest  
490 the wetland may be acting as a sink for mercury contamination in the upper and middle reaches.

491 This region of the wetland is hypoxic due to high decomposition rates of organic material, and  
492 mercury in low oxygen environments is transformed into methyl mercury, which is the form  
493 most toxic to living organisms (Hong et al., 2012; Sweet and Zelikoff, 2001). However, mercury  
494 can bioaccumulate within the food web and be present in toxic levels within piscivorous fish  
495 (Driscoll et al., 2007), which can be difficult to estimate from ambient environmental  
496 concentrations (Munthe et al., 2007). Because we did not directly measure mercury  
497 concentrations in fish, we cannot completely rule out the possibility of harmful levels of mercury  
498 within the food web.

499 Patterns of land use change in the basin are also reflected in increasing concentrations of C and  
500 N in wetland sediments over time, likely due to increased organic loading into the river. This  
501 pattern is generally mirrored by the C:N ratio, which can indicate the relative degree of aquatic  
502 or terrestrial production in the river (Cross et al., 2003; Kaushal and Binford, 1999). Terrestrial  
503 production that has entered the river typically has a higher C:N ratio, while aquatic production  
504 occurring within the river typically has a lower ratio. Thus, the increase and peak in C:N that  
505 occurs from ~1950-1970 and aligns with the increased percent of C and N loading likely  
506 indicates an influx of terrestrially-derived production entering the river as a result of  
507 deforestation and land cover change (Kaushal and Binford, 1999; Neill et al., 2001) (Figs. 9 and  
508 S9).

509 Both  $\delta^{13}\text{C}$  and  $\delta^{15}\text{N}$  were relatively stable over historical time scales from ~2000 years BP until  
510 significant anthropogenic change began occurring in the latter half of the 20<sup>th</sup> century (Fig. 9B).  
511 The general trend in the  $\delta^{13}\text{C}$  of organic carbon to more negative values may indicate increasing  
512 tree cover relative to grass cover on the landscape. Trees in this region are predominantly C3  
513 plants with a  $\delta^{13}\text{C}$  around -28‰, and savanna grasses are predominantly C4 plants with a  $\delta^{13}\text{C}$

514 around -14‰ (Masese et al., 2015; Masese et al., 2018). Some of this decline (~ 2‰) can also be  
515 explained by a negative shift in  $\delta^{13}\text{C}$  due to fossil fuels in the atmosphere (Cerling and Harris,  
516 1999; Francey et al., 1999). More complicated subsequent changes (between 1950-1990) could  
517 arise from a combination of factors. Significant changes in wildlife populations did occur during  
518 this time, and hippos in particular load large amounts of savanna grass into the river during daily  
519 feeding migrations (Subalusky et al., 2015). The earliest surveys of hippos in the Mara,  
520 conducted in 1959, showed very low numbers that were likely lower than historical abundances  
521 (Darling, 1960). Populations then increased exponentially in surveys conducted in 1971 (Olivier  
522 and Laurie, 1974) and 1980 (Karstad and Hudson, 1984), and then generally stabilized through  
523 2006 (Kanga et al., 2011). The apparent decrease and subsequent increase in organic C from  
524 savanna grasses might thus represent a lagged response to the decline and recovery of hippos.  
525 Other factors also may also contribute, including changes in plant community composition in the  
526 landscape and in the wetland, changing size of the wetland, and other landscape level patterns  
527 including increased burning and deforestation.

528 Changes in  $\delta^{15}\text{N}$  indicate an increase in anthropogenic nutrient loading into the river beginning  
529 in the 1960s and becoming more significant in the 1980s until stabilizing more recently. Other  
530 studies have shown that anthropogenic inputs (via agricultural runoff and sewage) are elevated in  
531 nitrogen, and that anthropogenic N is enriched in  $^{15}\text{N}$  producing elevated  $\delta^{15}\text{N}$  compared to non-  
532 anthropogenic sources (McClelland et al., 1997).

533 Changes in erosion processes throughout the basin were likely caused by significant changes in  
534 land use and land cover that were coincident with both the eradication of rinderpest and  
535 increasing deforestation in the basin. Rinderpest was first found in the Mara region in the 1890s  
536 (Percival, 1985) and decimated populations of wild and domestic animals; however, it had been

537 virtually eradicated by 1963 (Talbot and Talbot, 1963), likely due to the vaccination campaign of  
538 domestic animals by the local governments (Mariner et al., 2012) and the development of a  
539 natural immunity by wildebeest (Plowright and McCulloch, 1967; Sinclair, 1979; Taylor and  
540 Watson, 1967). The corresponding increase in livestock and wildlife in the mid-1960s also  
541 coincided with the beginning of legal and illegal settlements in the Mau Forest (Baldyga et al.,  
542 2008).

## 543 **5. Conclusions**

544 The Mara Wetland is influenced by changes in the Mara River basin and likely plays an  
545 important role in mitigating how those changes influence Lake Victoria. The wetland acts as a  
546 sediment trap, with sediment accumulating at higher rates in the Upper Wetland than the Lower  
547 Wetland. This wetland function has likely reduced the impact on Lake Victoria of increased  
548 sediment transport from the basin since the mid-1900s. Sediment deposition may have  
549 contributed to an increase in the size of the Mara Wetland that was proposed to have occurred in  
550 the mid-1900s (Mati et al., 2008). The Mara Wetland also appears to act as a sink for mercury  
551 contamination, as a large peak in mercury concentration in the Upper Wetland has yet to emerge  
552 in the Middle or Lower Wetland sites. Although retention of mercury in the wetland may  
553 positively impact the mercury concentrations reaching Lake Victoria, it does raise conservation  
554 and health concerns due to the potential transformation of mercury into methyl mercury, which is  
555 the form most toxic to people and animals (Hong et al., 2012).

556 We also observed that downstream effects of landcover and land use change can be significant  
557 and can be exacerbated by changing precipitation patterns (Nearing et al., 2005). Increasing  
558 extreme rainfall events have likely exacerbated the already increasing sedimentation rates within

559 the basin (Mango et al., 2011). Throughout East Africa, sedimentation has likely increased and  
560 will continue to increase as the region continues to receive a higher frequency of extreme rainfall  
561 events (Bartzke et al., 2018; Muthoni et al., 2018). Basin-wide historical changes we observed in  
562 the Mara Wetland cores are likely indicative of changes occurring throughout the region (Guzha  
563 et al., 2018) and provide a historical context to the consequences of increasing development  
564 coupled with increasing rainfall variability. Combining age-depth modelling with sediment  
565 fingerprinting can help reconstruct historical sedimentation patterns in the context of land use  
566 changes in understudied regions.

## 567 **Acknowledgements**

568 We thank the Republic of Kenya, the United Republic of Tanzania, Andrew McVey and WWF  
569 for helping initiate this research. We also thank the Musoma office of the Tanzanian Fisheries  
570 Surveillance Office for providing boats and assistance in the field. Mwasiti Rashid, Renata  
571 Montserrat, and Ella Jourdain provided assistance in the field and laboratory.

## 572 **Funding**

573 This work was supported by WWF-UK, WWF-Tanzania and WWF-Kenya Program Offices.  
574 Funding was also provided by grants from the National Science Foundation to DMP (DEB  
575 1354053 and 1753727) and EJR (DEB 1354062). The findings and conclusions in this article are  
576 those of the authors and do not necessarily represent the views of the U.S. National Park Service.

## 577 **References**

578 Abril JM, San Miguel EG, Ruiz-Canovas C, Casas-Ruiz M, Bolívar JP. From floodplain to  
579 aquatic sediments: Radiogeochronological fingerprints in a sediment core from the

580 mining impacted Sancho Reservoir (SW Spain). *Science of The Total Environment* 2018;  
581 631-632: 866-878; 10.1016/j.scitotenv.2018.03.114.

582 Aquino-López MA, Blaauw M, Christen JA, Sanderson NK. Bayesian Analysis of 210Pb  
583 Dating. *Journal of Agricultural, Biological and Environmental Statistics* 2018; 23: 317-  
584 333; 10.1007/s13253-018-0328-7.

585 Århem K, Fredén F. Land cover change and its influence on soil erosion in the Mara region,  
586 Tanzania: using satellite remote sensing and the Revised Universal Soil Loss Equation  
587 (RUSLE) to map land degradation between 1986 and 2013. Student thesis series INES  
588 2014

589 Arias-Ortiz A, Masqué P, Garcia-Orellana J, Serrano O, Mazarrasa I, Marbà N, et al. Reviews  
590 and syntheses: 210Pb-derived sediment and carbon accumulation rates in vegetated  
591 coastal ecosystems – setting the record straight. *Biogeosciences* 2018; 15: 6791-6818;  
592 10.5194/bg-15-6791-2018.

593 Bachmann WR, Hoyer VM, Canfield ED. Possible Sediment Mixing and the Disparity between  
594 Field Measurements and Paleolimnological Inferences in Shallow Iowa Lakes in the  
595 Midwestern United States. *Geosciences* 2018; 8; 10.3390/geosciences8020040.

596 Baldyga TJ, Miller SN, Driese KL, Gichaba CM. Assessing land cover change in Kenya's Mau  
597 Forest region using remotely sensed data. *African Journal of Ecology* 2008; 46: 46-54;  
598 10.1111/j.1365-2028.2007.00806.x.

599 Bartzke GS, Ogotu JO, Mukhopadhyay S, Mtui D, Dublin HT, Piepho H-P. Rainfall trends and  
600 variation in the Maasai Mara ecosystem and their implications for animal population and  
601 biodiversity dynamics. *PLOS ONE* 2018; 13: e0202814; 10.1371/journal.pone.0202814.

602 Baskaran M, Nix J, Kuyper C, Karunakara N. Problems with the dating of sediment core using  
603 excess  $^{210}\text{Pb}$  in a freshwater system impacted by large scale watershed changes. *Journal*  
604 *of Environmental Radioactivity* 2014; 138: 355-363; 10.1016/j.jenvrad.2014.07.006.

605 Bavor HJ, Waters MT. Buffering Performance in a Papyrus-Dominated Wetland System of the  
606 Kenyan Portion of the Lake Victoria Basin. In: Vymazal J, editor. *Wastewater Treatment,*  
607 *Plant Dynamics and Management in Constructed and Natural Wetlands.* Springer  
608 Netherlands, Dordrecht, 2008, pp. 33-38; 10.1007/978-1-4020-8235-1\_4.

609 Benoit G, Rozan TF.  $^{210}\text{Pb}$  and  $^{137}\text{Cs}$  dating methods in lakes: a retrospective study. *Journal of*  
610 *Paleolimnology* 2001; 25: 455-465; 10.1023/A:1011179318352.

611 Blaauw M, Christen JA. Flexible paleoclimate age-depth models using an autoregressive gamma  
612 process. *Bayesian Analysis* 2011; 6: 457-474; 10.1214/11-BA618.

613 Blake WH, Boeckx P, Stock BC, Smith HG, Bodé S, Upadhayay HR, et al. A deconvolutional  
614 Bayesian mixing model approach for river basin sediment source apportionment.  
615 *Scientific Reports* 2018; 8: 13073; 10.1038/s41598-018-30905-9.

616 Bronk Ramsey C. Radiocarbon Dating: Revolutions in Understanding. *Archaeometry* 2008; 50:  
617 249-275; 10.1111/j.1475-4754.2008.00394.x.

618 Cerling TE, Harris JM. Carbon isotope fractionation between diet and bioapatite in ungulate  
619 mammals and implications for ecological and paleoecological studies. *Oecologia* 1999;  
620 120: 347-363; 10.1007/s004420050868.

621 Christen JA, Fox C. A general purpose sampling algorithm for continuous distributions (the t -  
622 walk). *Bayesian Analysis* 2010; 5: 263-281; 10.1214/10-BA603.

623 Collins AL, Pulley S, Foster IDL, Gellis A, Porto P, Horowitz AJ. Sediment source  
624 fingerprinting as an aid to catchment management: A review of the current state of

625 knowledge and a methodological decision-tree for end-users. *Journal of Environmental*  
626 *Management* 2017; 194: 86-108; 10.1016/j.jenvman.2016.09.075.

627 Comans RNJ, Middelburg JJ, Zonderhuis J, Woittiez JRW, Lange GJD, Das HA, et al.  
628 Mobilization of radiocaesium in pore water of lake sediments. *Nature* 1989; 339: 367;  
629 10.1038/339367a0.

630 Cross WF, Benstead JP, Rosemond AD, Bruce Wallace J. Consumer-resource stoichiometry in  
631 detritus-based streams. *Ecology Letters* 2003; 6: 721-732; 10.1046/j.1461-  
632 0248.2003.00481.x.

633 Cutshall NH, Larsen IL, Olsen CR. Direct analysis of Pb-210 in sediment samples: Self-  
634 absorption corrections. *Nuclear Instruments and Methods* 1983; 206: 309-312

635 Darling FF. *An Ecological Reconnaissance of the Mara Plains in Kenya Colony*. *Wildlife*  
636 *Monographs* 1960: 3-41

637 Davis RB, Hess CT, Norton SA, Hanson DW, Hoagland KD, Anderson DS. <sup>137</sup>Cs and <sup>210</sup>Pb  
638 dating of sediments from soft-water lakes in New England (USA) and Scandinavia, a  
639 failure of <sup>137</sup>Cs dating. *Chemical Geology* 1984; 44: 151-185; 10.1016/0009-  
640 2541(84)90071-8.

641 Defersha MB, Melesse AM, McClain ME. Watershed scale application of WEPP and EROSION  
642 3D models for assessment of potential sediment source areas and runoff flux in the Mara  
643 River Basin, Kenya. *Catena* 2012; 95: 63-72; 10.1016/j.catena.2012.03.004.

644 Drexler JZ, Fuller CC, Archfield S. The approaching obsolescence of <sup>137</sup>Cs dating of wetland  
645 soils in North America. *Quaternary Science Reviews* 2018; 199: 83-96;  
646 10.1016/j.quascirev.2018.08.028.

647 Driscoll CT, Han Y-J, Chen CY, Evers DC, Lambert KF, Holsen TM, et al. Mercury  
648 Contamination in Forest and Freshwater Ecosystems in the Northeastern United States.  
649 BioScience 2007; 57: 12

650 Dutton C, Anisfeld S, Ernstberger H. A novel sediment fingerprinting method using filtration:  
651 application to the Mara River, East Africa. Journal of Soils and Sediments 2013; 13:  
652 1708-1723; 10.1007/s11368-013-0725-z.

653 Dutton CL, Subalusky AL, Anisfeld SC, Njoroge L, Rosi EJ, Post DM. The influence of a semi-  
654 arid sub-catchment on suspended sediments in the Mara River, Kenya. PLOS ONE 2018;  
655 13: e0192828; 10.1371/journal.pone.0192828.

656 Dutton CL, Subalusky AL, Hill TD, Aleman JC, Rosi EJ, Onyango KB, et al. Data for: A 2000-  
657 year sediment record reveals rapidly changing sedimentation and land use since the 1960s  
658 in the Upper Mara-Serengeti Ecosystem. Mendeley Data. v1, 2019;  
659 10.17632/vfd5vzm6rm.1.

660 FAO. FAOSTAT statistics database. FAO, 2018, 2018.

661 Foley JA, DeFries R, Asner GP, Barford C, Bonan G, Carpenter SR, et al. Global Consequences  
662 of Land Use. Science 2005; 309: 570-574; 10.1126/science.1111772.

663 Francey RJ, Allison CE, Etheridge DM, Trudinger CM, Enting IG, Leuenberger M, et al. A  
664 1000-year high precision record of  $\delta^{13}\text{C}$  in atmospheric  $\text{CO}_2$ . Tellus B 1999; 51: 170-  
665 193; 10.1034/j.1600-0889.1999.t01-1-00005.x.

666 Gamby RL, Hammerschmidt CR, Costello DM, Lamborg CH, Runkle JR. Deforestation and  
667 cultivation mobilize mercury from topsoil. Science of The Total Environment 2015; 532:  
668 467-473; 10.1016/j.scitotenv.2015.06.025.

669 Guzha AC, Rufino MC, Okoth S, Jacobs S, Nóbrega RLB. Impacts of land use and land cover  
670 change on surface runoff, discharge and low flows: Evidence from East Africa. Journal of  
671 Hydrology: Regional Studies 2018; 15: 49-67; 10.1016/j.ejrh.2017.11.005.

672 Haslett J, Parnell A. A simple monotone process with application to radiocarbon-dated depth  
673 chronologies. Journal of the Royal Statistical Society: Series C (Applied Statistics) 2008;  
674 57: 399-418; 10.1111/j.1467-9876.2008.00623.x.

675 Hoffman CM. Geospatial mapping and analysis of water availability-demand-use within the  
676 Mara River Basin. Msc. Florida International University, Miami, 2007.

677 Holdo RM, Holt RD, Fryxell JM. Opposing Rainfall and Plant Nutritional Gradients Best  
678 Explain the Wildebeest Migration in the Serengeti. The American Naturalist 2009; 173:  
679 431-445; 10.1086/597229.

680 Hong Y-S, Kim Y-M, Lee K-E. Methylmercury exposure and health effects. Journal of  
681 preventive medicine and public health = Yebang Uihakhoe chi 2012; 45: 353-363;  
682 10.3961/jpmp.2012.45.6.353.

683 Hopcraft JGC, Sinclair ARE, Holdo RM, Mwangomo E, Mduma S, Thirgood S, et al. Why are  
684 wildebeest the most abundant herbivore in the Serengeti ecosystem? Serengeti IV:  
685 Sustaining Biodiversity in a Coupled Human–Natural System. University of Chicago  
686 Press, Chicago, Illinois, USA, 2013

687 Jaschinski S, Hansen T, Sommer U. Effects of acidification in multiple stable isotope analyses.  
688 Limnology and Oceanography: Methods 2008; 6: 12-15; 10.4319/lom.2008.6.12.

689 Kanga EM, Ogutu JO, Oloff H, Santema P. Population trend and distribution of the vulnerable  
690 common hippopotamus *Hippopotamus amphibius* in the Mara Region of Kenya. Oryx  
691 2011; 45: 20-27

692 Kansiime F, Saunders MJ, Loiselle SA. Functioning and dynamics of wetland vegetation of Lake  
693 Victoria: an overview. *Wetlands Ecology and Management* 2007; 15: 443-451;  
694 10.1007/s11273-007-9043-9.

695 Karstad EL, Hudson RJ. Census of the Mara River hippopotamus (*Hippopotamus amphibius*),  
696 southwest Kenya, 1980–1982. *African Journal of Ecology* 1984; 22: 143-147;  
697 10.1111/j.1365-2028.1984.tb00687.x.

698 Kassenga GR. A descriptive assessment of the wetlands of the Lake Victoria basin in Tanzania.  
699 *Resources, Conservation and Recycling* 1997; 20: 127-141; 10.1016/S0921-  
700 3449(97)00014-1.

701 Kaushal S, Binford MW. Relationship between C:N ratios of lake sediments, organic matter  
702 sources, and historical deforestation in Lake Pleasant, Massachusetts, USA. *Journal of*  
703 *Paleolimnology* 1999; 22: 439-442; 10.1023/a:1008027028029.

704 Kemp AC, Horton BP, Vane CH, Bernhardt CE, Corbett DR, Engelhart SE, et al. Sea-level  
705 change during the last 2500 years in New Jersey, USA. *Quaternary Science Reviews*  
706 2013; 81: 90-104; 10.1016/j.quascirev.2013.09.024.

707 Kirchner G. <sup>210</sup>Pb as a tool for establishing sediment chronologies: examples of potentials and  
708 limitations of conventional dating models. *Journal of Environmental Radioactivity* 2011;  
709 102: 490-494; 10.1016/j.jenvrad.2010.11.010.

710 Kruskal WH, Wallis WA. Use of Ranks in One-Criterion Variance Analysis. *Journal of the*  
711 *American Statistical Association* 1952; 47: 583-621; 10.1080/01621459.1952.10483441.

712 Kundzewicz ZW. Water resources for sustainable development. *Hydrological Sciences Journal*  
713 1997; 42: 467-480; 10.1080/02626669709492047.

714 LVBC, WWF-ESARPO. Assessing Reserve Flows for the Mara River, Kenya and Tanzania.  
715 Lake Victoria Basin Commission of the East African Community, Kisumu, 2010.

716 Mabit L, Benmansour M, Abril JM, Walling DE, Meusburger K, Iurian AR, et al. Fallout 210Pb  
717 as a soil and sediment tracer in catchment sediment budget investigations: A review.  
718 Earth-Science Reviews 2014; 138: 335-351; 10.1016/j.earscirev.2014.06.007.

719 Mango LM, Melesse AM, McClain ME, Gann D, Setegn SG. Land use and climate change  
720 impacts on the hydrology of the upper Mara River Basin, Kenya: results of a modeling  
721 study to support better resource management. Hydrology and Earth System Sciences  
722 2011; 15: 2245-2258

723 Mariner JC, House JA, Mebus CA, Sollod AE, Chibeu D, Jones BA, et al. Rinderpest  
724 Eradication: Appropriate Technology and Social Innovations. Science 2012; 337: 1309-  
725 1312; 10.1126/science.1223805.

726 Masese FO, Abrantes KG, Gettel GM, Bouillon S, Irvine K, McClain ME. Are Large Herbivores  
727 Vectors of Terrestrial Subsidies for Riverine Food Webs? Ecosystems 2015; 18: 686-706;  
728 10.1007/s10021-015-9859-8.

729 Masese FO, Abrantes KG, Gettel GM, Irvine K, Bouillon S, McClain ME. Trophic structure of  
730 an African savanna river and organic matter inputs by large terrestrial herbivores: A  
731 stable isotope approach. Freshwater Biology 2018; 0; doi:10.1111/fwb.13163.

732 Mati BM, Mutie S, Gadain H, Home P, Mtalo F. Impacts of land-use/cover changes on the  
733 hydrology of the transboundary Mara River, Kenya/Tanzania. Lakes & Reservoirs:  
734 Research & Management 2008; 13: 169-177; 10.1111/j.1440-1770.2008.00367.x.

735 Mayo AW, Muraza M, Norbert J. The role of Mara River Basin Wetland in reduction of nitrogen  
736 load to Lake Victoria. *International Journal of Water Resources and Environmental*  
737 *Engineering* 2013; 5: 659-669; 10.5897/IJWREE2013.0444.

738 McClain ME. Balancing Water Resources Development and Environmental Sustainability in  
739 Africa: A Review of Recent Research Findings and Applications. *AMBIO* 2013; 42: 549-  
740 565; 10.1007/s13280-012-0359-1.

741 McClain ME, Subalusky AL, Anderson EP, Dessu SB, Melesse AM, Ndomba PM, et al.  
742 Comparing flow regime, channel hydraulics, and biological communities to infer flow–  
743 ecology relationships in the Mara River of Kenya and Tanzania. *Hydrological Sciences*  
744 *Journal* 2014; 59: 801-819; 10.1080/02626667.2013.853121.

745 McClelland JW, Valiela I, Michener RH. Nitrogen-stable isotope signatures in estuarine food  
746 webs: A record of increasing urbanization in coastal watersheds. *Limnology and*  
747 *Oceanography* 1997; 42: 930-937; 10.4319/lo.1997.42.5.0930.

748 Mduma SAR, Sinclair ARE, Hilborn R. Food regulates the Serengeti wildebeest: a 40-year  
749 record. *Journal of Animal Ecology* 1999; 68: 1101-1122; 10.1046/j.1365-  
750 2656.1999.00352.x.

751 Moore JW, Semmens BX. Incorporating uncertainty and prior information into stable isotope  
752 mixing models. *Ecology Letters* 2008; 11: 470-480; 10.1111/j.1461-0248.2008.01163.x.

753 Munthe J, Bodaly RA, Branfireun BA, Driscoll CT, Gilmour CC, Harris R, et al. Recovery of  
754 Mercury-Contaminated Fisheries. *Ambio* 2007; 36: 12

755 Muthoni FK, Odongo VO, Ochieng J, Mugalavai EM, Mourice SK, Hoesche-Zeledon I, et al.  
756 Long-term spatial-temporal trends and variability of rainfall over Eastern and Southern  
757 Africa. *Theoretical and Applied Climatology* 2018; 10.1007/s00704-018-2712-1.

758 Mwangi MH, Lariu P, Julich S, Patil DS, McDonald AM, Feger K-H. Characterizing the  
759 Intensity and Dynamics of Land-Use Change in the Mara River Basin, East Africa.  
760 Forests 2018; 9; 10.3390/f9010008.

761 Nearing MA, Jetten V, Baffaut C, Cerdan O, Couturier A, Hernandez M, et al. Modeling  
762 response of soil erosion and runoff to changes in precipitation and cover. CATENA 2005;  
763 61: 131-154; 10.1016/j.catena.2005.03.007.

764 Neill C, Deegan LA, Thomas SM, Cerri CC. Deforestation for Pasture Alters Nitrogen and  
765 Phosphorus in Small Amazonian Streams. Ecological Applications 2001; 11: 1817-1828;  
766 10.2307/3061098.

767 Nyarko E, Klubi E, Laissaoui A, Benmansour M. Estimating recent sedimentation rates using  
768 lead-210 in tropical estuarine systems: case study of Volta and Pra estuaries in Ghana,  
769 West Africa. Journal of Oceanography and Marine Research 2016; 10.4172/2572-  
770 3103.1000141.

771 O'Sullivan JJ, Lupakisyo Mwalwiba G, Purcell PJ, Turner JN, Mtalo F. Assessing sediment and  
772 water quality issues in expanding African wetlands: the case of the Mara River, Tanzania.  
773 International Journal of Environmental Studies 2016; 73: 95-107;  
774 10.1080/00207233.2015.1116226.

775 Odada EO, Olago DO, Kulindwa K, Ntiba M, Wandiga S. Mitigation of Environmental  
776 Problems in Lake Victoria, East Africa: Causal Chain and Policy Options Analyses.  
777 AMBIO: A Journal of the Human Environment 2004; 33: 13-23; 10.1579/0044-7447-  
778 33.1.13.

779 Ogutu JO, Owen-Smith N, Piepho HP, Said MY. Continuing wildlife population declines and  
780 range contraction in the Mara region of Kenya during 1977–2009. *Journal of Zoology*  
781 2011; 285: 99-109; 10.1111/j.1469-7998.2011.00818.x.

782 Ogutu JO, Piepho H-P, Said MY, Ojwang GO, Njino LW, Kifugo SC, et al. Extreme Wildlife  
783 Declines and Concurrent Increase in Livestock Numbers in Kenya: What Are the Causes?  
784 PLOS ONE 2016; 11: e0163249; 10.1371/journal.pone.0163249.

785 Olang LO, Kundu PM. Land degradation of the Mau forest complex in Eastern Africa: a review  
786 for management and restoration planning. *Environmental Monitoring. InTech*, 2011

787 Oldfield F, Appleby PG. Empirical testing of <sup>210</sup>Pb-dating models for lake sediments. In:  
788 Haworth EY, Lund JWG, editors. *Lake Sediments and Environmental History*. University  
789 of Minnesota, Minneapolis, MN, 1984, pp. 93-124

790 Olivier RCD, Laurie WA. Habitat utilization by hippopotamus in the Mara River\*. *African*  
791 *Journal of Ecology* 1974; 12: 249-271; 10.1111/j.1365-2028.1974.tb01036.x.

792 Parnell AC. *Bchron: Radiocarbon Dating, Age-Depth Modelling, Relative Sea Level Rate*  
793 *Estimation, and Non-Parametric Phase Modelling*, 2016.

794 Percival AB. *A game ranger on safari*. Clinton, N.J.: Amwell Press, 1985

795 Plowright W, McCulloch B. Investigations on the incidence of rinderpest virus infection in game  
796 animals of N. Tanganyika and S. Kenya 1960/63. *Epidemiology & Infection* 1967; 65:  
797 343-358

798 R Core Team. *R: A language and environment for statistical computing*. R Foundation for  
799 *Statistical Computing*, Vienna, Austria, 2018.

800 Raikes PL. *Livestock development and policy in East Africa*: Nordic Africa Institute, 1981

801 Ramnarine R, Voroney RP, Wagner-Riddle C, Dunfield KE. Carbonate removal by acid  
802 fumigation for measuring the  $\delta^{13}\text{C}$  of soil organic carbon. *Canadian Journal of Soil*  
803 *Science* 2011; 91: 247-250; 10.4141/cjss10066.

804 Reimer PJ, Bard E, Bayliss A, Beck JW, Blackwell PG, Ramsey CB, et al. IntCal13 and  
805 Marine13 radiocarbon age calibration curves 0–50,000 years cal BP. *Radiocarbon* 2013;  
806 55: 1869-1887; 10.2458/azu\_js\_rc.55.16947.

807 Ritchie JC, McHenry JR. Application of Radioactive Fallout Cesium-137 for Measuring Soil  
808 Erosion and Sediment Accumulation Rates and Patterns: A Review. *Journal of*  
809 *Environmental Quality* 1990; 19: 215-233; 10.2134/jeq1990.00472425001900020006x.

810 Robbins JA. Geochemical and geophysical applications of radioactive lead. In: Nriagu JO,  
811 editor. *Biogeochemistry of lead in the environment*. Elsevier, 1978, pp. 285-393

812 Roulet M, Lucotte M, Canuel R, Farella N, Courcelles M, Guimarães JRD, et al. Increase in  
813 mercury contamination recorded in lacustrine sediments following deforestation in the  
814 central Amazon! The present investigation is part of an ongoing study, the CARUSO  
815 project (CRDI-UFPa-UQAM), initiated to determine the sources, fate and health effects  
816 of the presence of MeHg in the area of the Lower Tapajós.1. *Chemical Geology* 2000;  
817 165: 243-266; 10.1016/S0009-2541(99)00172-2.

818 RStudio Team. *RStudio: Integrated Development for R*. RStudio, Inc., Boston, MA, 2016.

819 Saldarriaga-Isaza A, Villegas-Palacio C, Arango S. Phasing out mercury through collective  
820 action in artisanal gold mining: Evidence from a framed field experiment. *Ecological*  
821 *Economics* 2015; 120: 406-415; 10.1016/j.ecolecon.2015.04.004.

822 Scheren PAGM, Zanting HA, Lemmens AMC. Estimation of water pollution sources in Lake  
823 Victoria, East Africa: Application and elaboration of the rapid assessment methodology.  
824 Journal of Environmental Management 2000; 58: 235-248; 10.1006/jema.2000.0322.

825 Schwesig D, Ilgen G, Matzner E. Mercury and methylmercury in upland and wetland acid forest  
826 soils of a watershed in NE-Bavaria, Germany. Water, Air, and Soil Pollution 1999; 113:  
827 141-154

828 Sharma NP, Damhaug T, Gilgan-Hunt E, Grey D, Okaru V, Rothberg D. African Water  
829 Resources; Challenges and Opportunities for Sustainable Development, 1996.

830 Shillington K. History of Africa. London; New York, NY: Palgrave Macmillan, 2012

831 Sinclair A. The eruption of the ruminants. Serengeti: dynamics of an ecosystem 1979: 82-103

832 Smith JN. Why should we believe  $^{210}\text{Pb}$  sediment geochronologies? Journal of Environmental  
833 Radioactivity 2001; 55: 121-123; 10.1016/S0265-931X(00)00152-1.

834 Stock BC, Jackson AL, Ward EJ, Parnell AC, Phillips DL, Semmens BX. Analyzing mixing  
835 systems using a new generation of Bayesian tracer mixing models. PeerJ 2018; 6: e5096;  
836 10.7717/peerj.5096.

837 Stock BC, Semmens BX. MixSIAR GUI User Manual, 2016.

838 Subalusky AL, Dutton CL, Rosi-Marshall EJ, Post DM. The hippopotamus conveyor belt:  
839 vectors of carbon and nutrients from terrestrial grasslands to aquatic systems in sub-  
840 Saharan Africa. Freshwater Biology 2015; 60; 10.1111/fwb.12474.

841 Subalusky AL, Dutton CL, Rosi EJ, Post DM. Annual mass drownings of the Serengeti  
842 wildebeest migration influence nutrient cycling and storage in the Mara River.  
843 Proceedings of the National Academy of Sciences 2017; 114: 7647-7652;  
844 10.1073/pnas.1614778114.

845 Sweet LI, Zelikoff JT. Toxicology and immunotoxicology of mercury: A comparative review in  
846 fish and humans. *Journal of Toxicology and Environmental Health, Part B* 2001; 4: 161-  
847 205; 10.1080/10937400117236.

848 Talbot LM, Talbot MH. The Wildebeest in Western Masailand, East Africa. *Wildlife*  
849 *Monographs* 1963: 3-88

850 Taylor W, Watson RM. Studies on the epizootiology of rinderpest in blue wildebeest and other  
851 game species of Northern Tanzania and Southern Kenya, 1965–7. *Epidemiology &*  
852 *Infection* 1967; 65: 537-545

853 Telmer KH, Veiga MM. World emissions of mercury from artisanal and small scale gold mining.  
854 In: Mason R, Pirrone N, editors. *Mercury Fate and Transport in the Global Atmosphere:*  
855 *Emissions, Measurements and Models*. Springer US, Boston, MA, 2009, pp. 131-172;  
856 10.1007/978-0-387-93958-2\_6.

857 Turekian KK, Benninger LK, Dion EP. <sup>7</sup>Be and <sup>210</sup>Pb total deposition fluxes at New Haven,  
858 Connecticut and at Bermuda. *Journal of Geophysical Research: Oceans* 1983; 88: 5411-  
859 5415; 10.1029/JC088iC09p05411

860 UN-Water A. *The Africa Water Vision for 2025: Equitable and sustainable use of water for*  
861 *socioeconomic development*. 2003

862 Vanderkelen I, van Lipzig NPM, Thiery W. Modelling the water balance of Lake Victoria (East  
863 Africa) – Part 1: Observational analysis. *Hydrol. Earth Syst. Sci.* 2018; 22: 5509-5525;  
864 10.5194/hess-22-5509-2018.

865 Venables WN, Ripley BD. *Modern applied statistics with S*. New York: Springer, 2002;  
866 10.1007/978-0-387-21706-2.

867 Vörösmarty CJ, Green P, Salisbury J, Lammers RB. Global Water Resources: Vulnerability from  
868 Climate Change and Population Growth. *Science* 2000; 289: 284-288;  
869 10.1126/science.289.5477.284.

870 Wallbrink PJ, Murray AS, Olley JM, Olive LJ. Determining sources and transit times of  
871 suspended sediment in the Murrumbidgee River, New South Wales, Australia, using  
872 fallout <sup>137</sup>Cs and <sup>210</sup>Pb. *Water Resources Research* 1998; 34: 879-887;  
873 10.1029/97WR03471.

874 Walling DE, Owens PN, Carter J, Leeks GJL, Lewis S, Meharg AA, et al. Storage of sediment-  
875 associated nutrients and contaminants in river channel and floodplain systems. *Applied*  
876 *Geochemistry* 2003; 18: 195-220; 10.1016/S0883-2927(02)00121-X.

877 Wang J, Baskaran M, Niedermiller J. Mobility of <sup>137</sup>Cs in freshwater lakes: A mass balance and  
878 diffusion study of Lake St. Clair, Southeast Michigan, USA. *Geochimica et*  
879 *Cosmochimica Acta* 2017; 218: 323-342; 10.1016/j.gca.2017.09.017.

880 Weihs C, Ligges U, Luebke K, Raabe N. klaR Analyzing German Business Cycles. In: Baier D,  
881 Decker R, Schmidt-Thieme L, editors. *Data Analysis and Decision Support*. Springer-  
882 Verlag, Berlin, 2005, pp. 335-343; 10.1007/3-540-28397-8\_36.

883

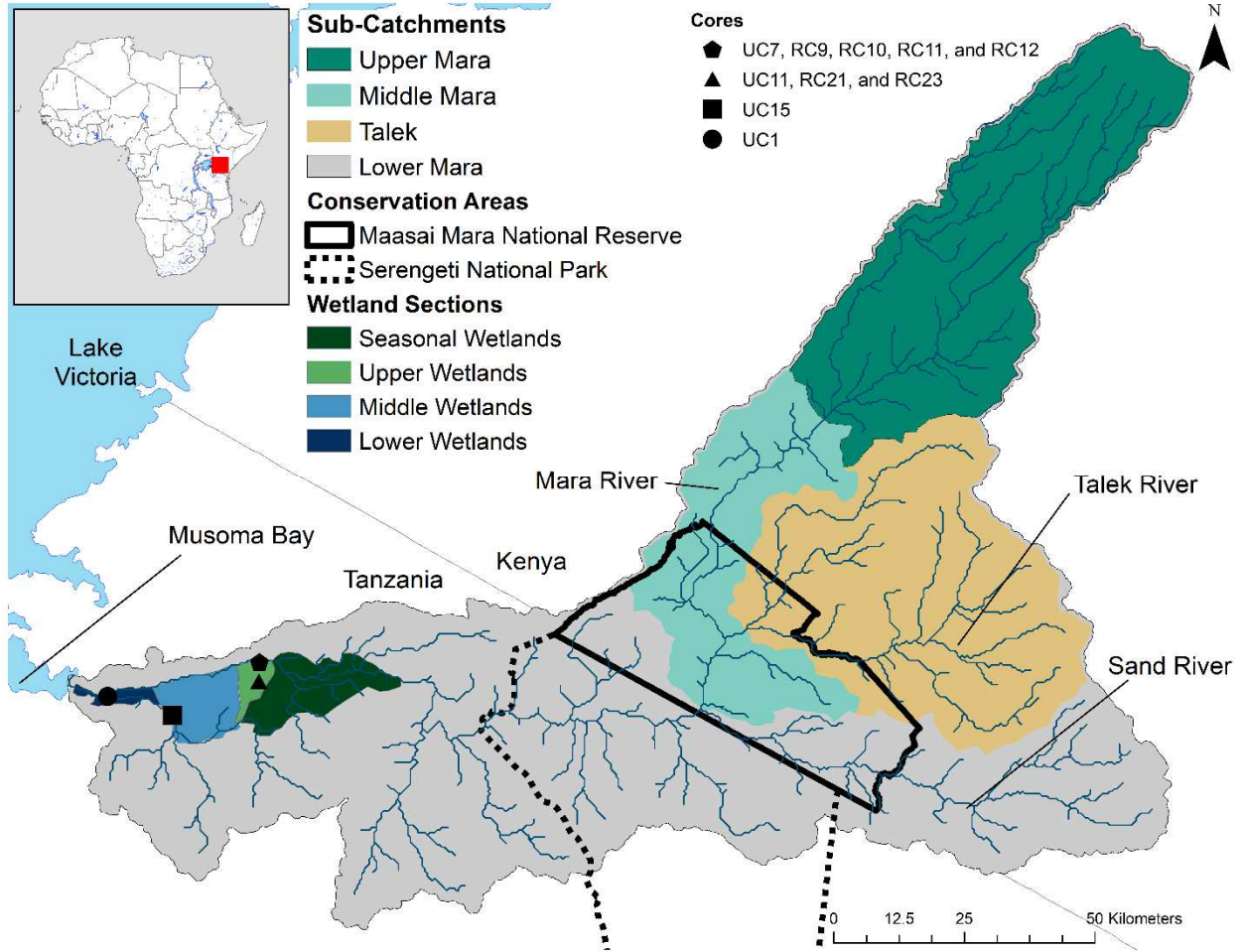


Figure 1. The Mara River basin is a trans-boundary basin shared between Kenya and Tanzania. Sediment source fingerprints were developed for the four sub-catchments. Sediment cores were collected to represent the four sections of the Mara Wetland.

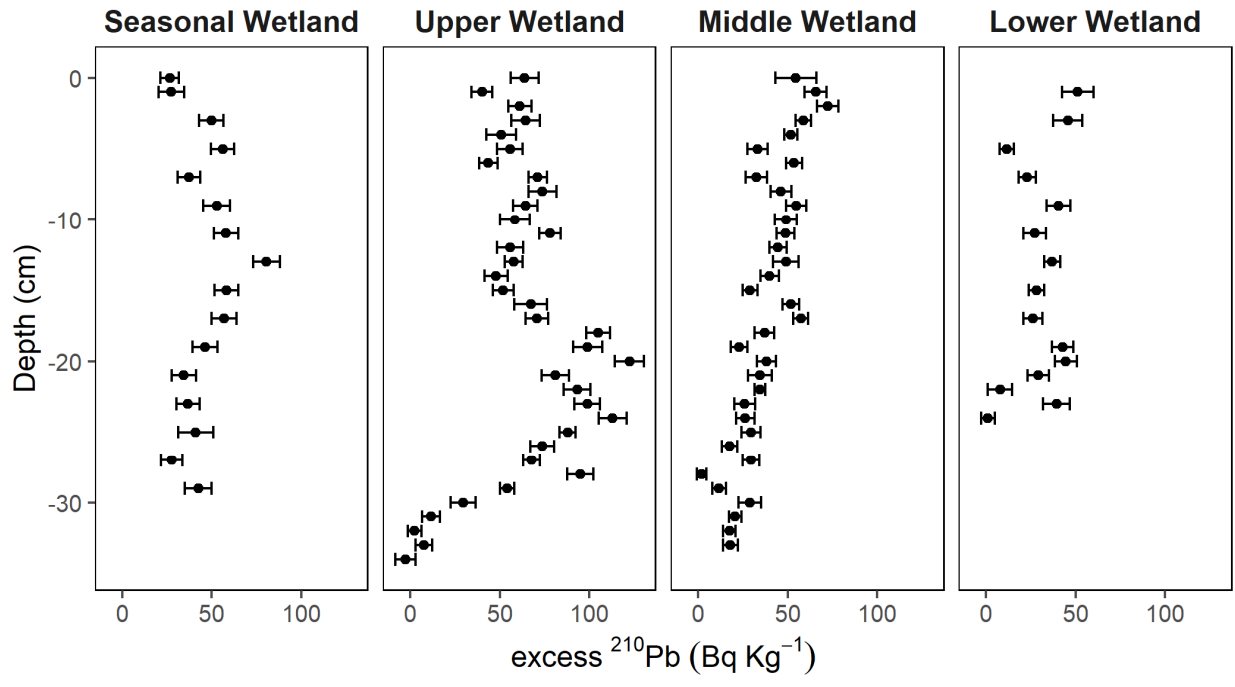


Figure 2. Excess <sup>210</sup>Pb concentrations (mean and standard deviation) for the four cores (Seasonal Wetland, Upper Wetland, Middle Wetland, and Lower Wetland).

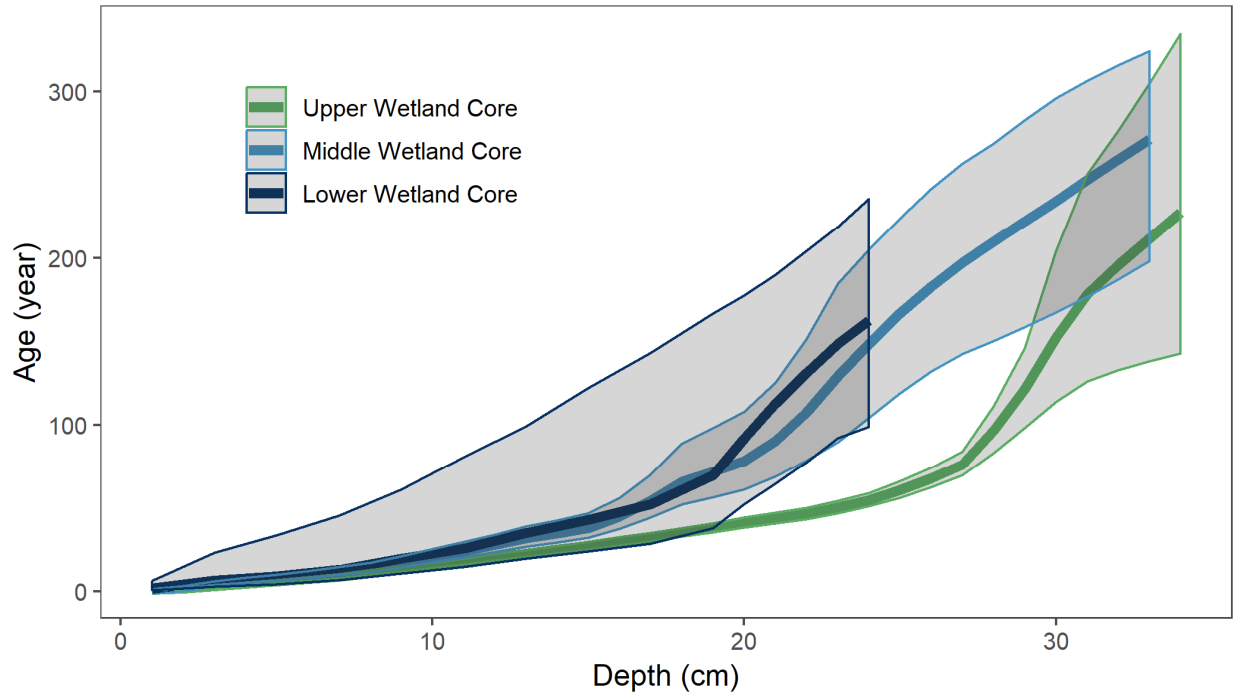


Figure 3. Plum Bayesian age-depth models for the Upper Wetland core (light green), Middle Wetland core (light blue) and Lower Wetland core (dark blue). Shaded area represents 95% confidence region. Colors match the wetland regions represented in Figure 1.

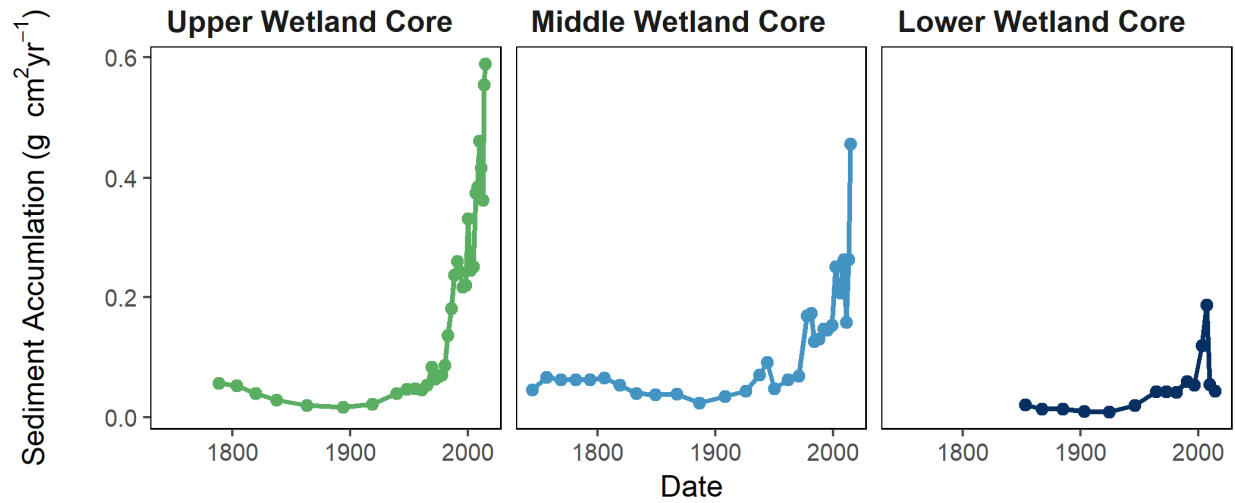


Figure 4. Sediment accumulation chronologies in cores from a lake in the Upper Wetland (UC11, left column), the Middle Wetland (UC15, middle column) and the Lower Wetland near Lake Victoria (UC1, right column) using the Plum model. Colors match the wetland regions represented in Figure 1.

## Upper Wetland Age-Depth Model

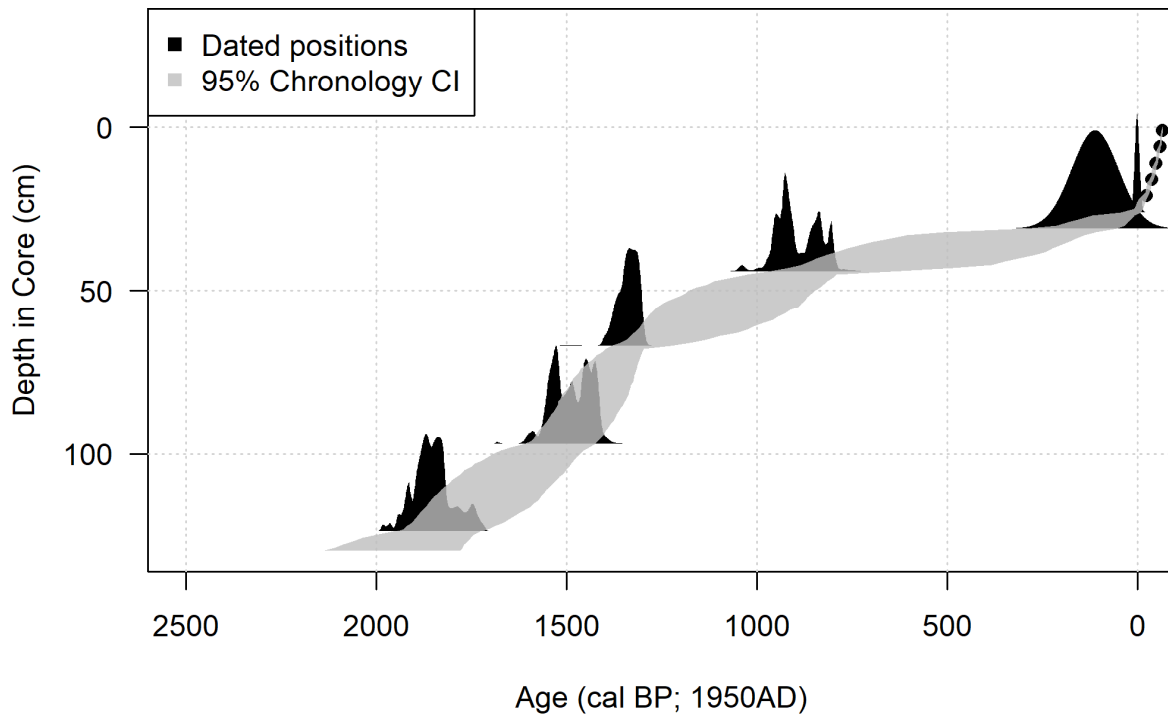


Figure 5. Bayesian age-depth model for the Upper Wetland core set (UC11, RC21, and RC23) using radiocarbon and  $^{210}\text{Pb}$  dating. Points and the two density probability curves on the right represent the  $^{210}\text{Pb}$  dates from the Plum Bayesian age-depth model (taken every 5 cm, 7 dates total); radiocarbon dates are represented as the four density of probability curves on the left (Parnell, 2016). Age in 'cal BP' refers to the age in calibrated years before present, the present being 1950 by convention.

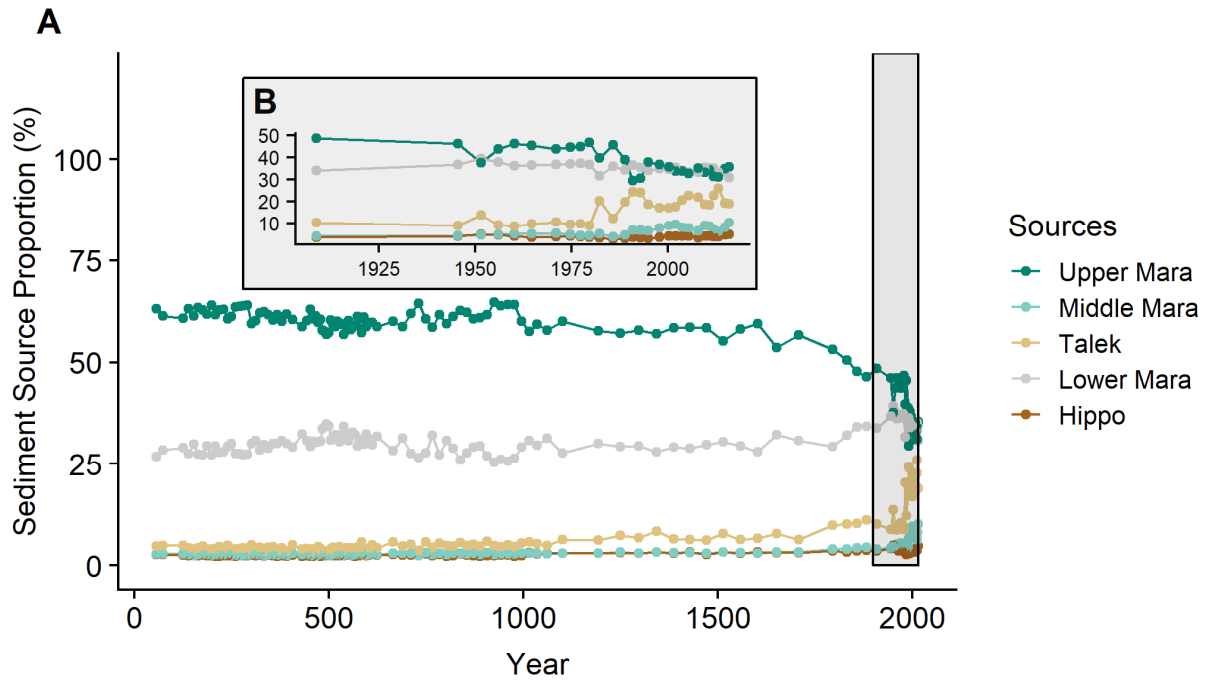


Figure 6. **A.** Sediment fingerprinting source proportion in the Upper Wetland set of cores (UC11, RC21, RC23) for approximately 2000 years. Source proportions from 1900 to present day highlighted in gray. **B.** Source proportions from 1900 to present day. Colors match the regions represented in Figure 1.

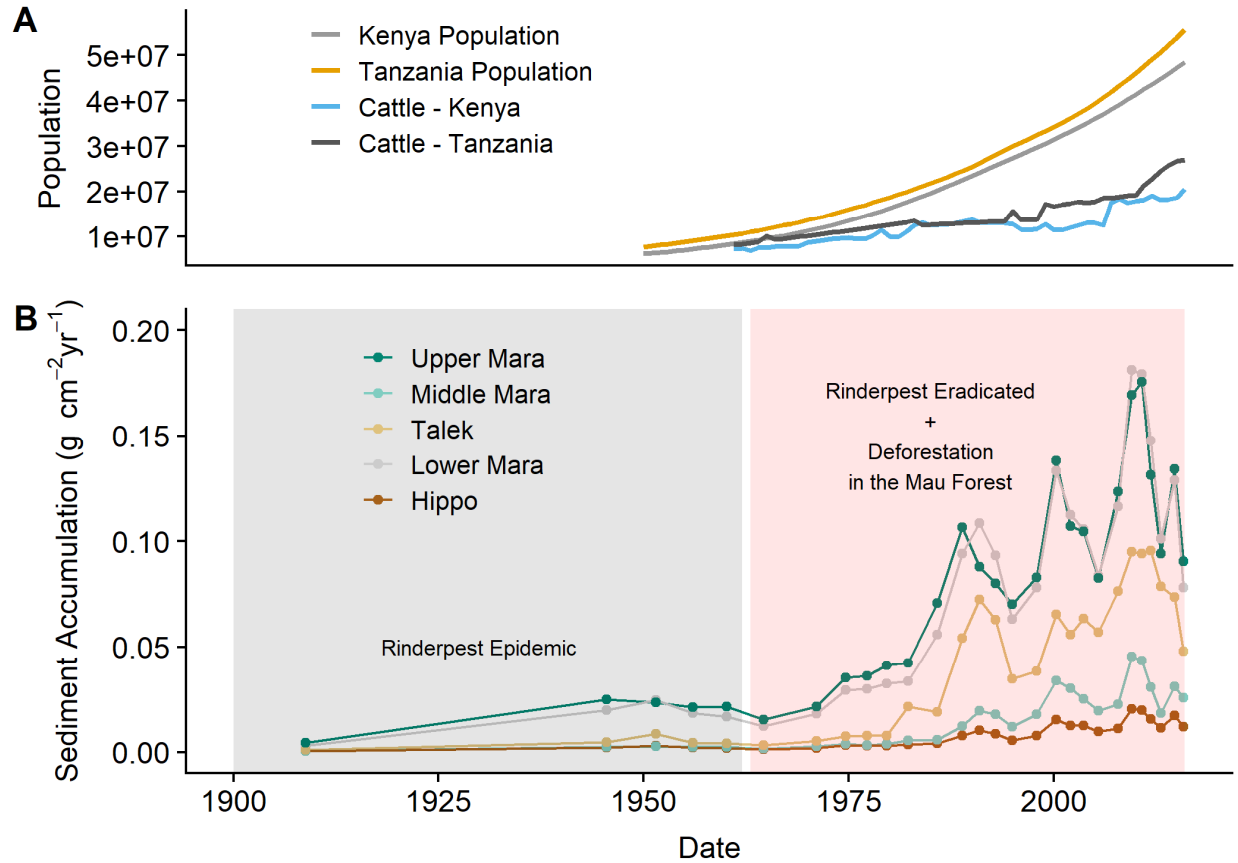


Figure 7. **A.** Kenya and Tanzania human population and cattle population numbers from 1950 to present (FAO, 2018). **B.** Sediment accumulation from 1900 to present day in the Upper Wetland Core (UC11). Colors match the regions represented in Figure 1. Gray box indicates the time of the rinderpest epidemic in the Mara-Serengeti (~1894-1962) (Talbot and Talbot, 1963). Red box indicates the eradication of Rinderpest in the Mara-Serengeti and the deforestation in the Mau Forest (~1964-Present) (Baldyga et al., 2008; Talbot and Talbot, 1963).

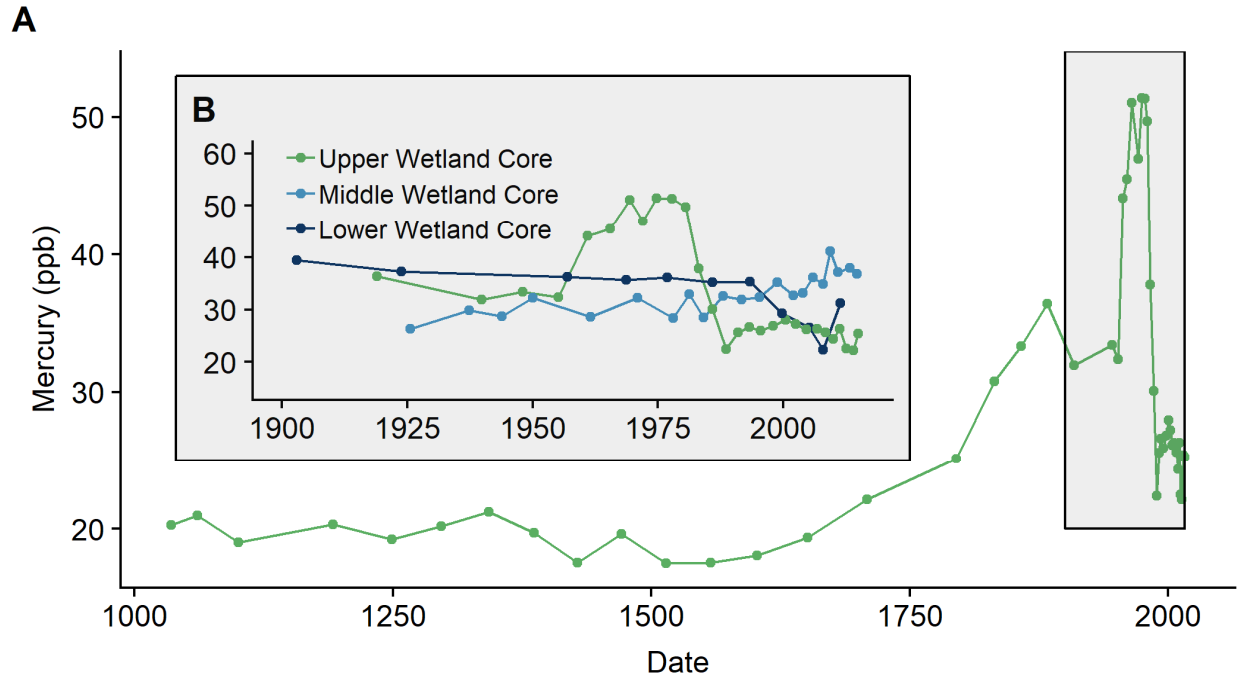


Figure 8. **A.** Mercury concentration (in parts per billion) in a sediment core from the Upper Wetland from 1100 AD to present day. Mercury concentrations from 1900 to the present day highlighted in the gray box. **B.** Mercury concentrations (in parts per billion) from the Upper Wetland (red), Middle Wetland (orange) and Lower Wetland (blue) sediment cores. Colors match the regions represented in Figure 1.

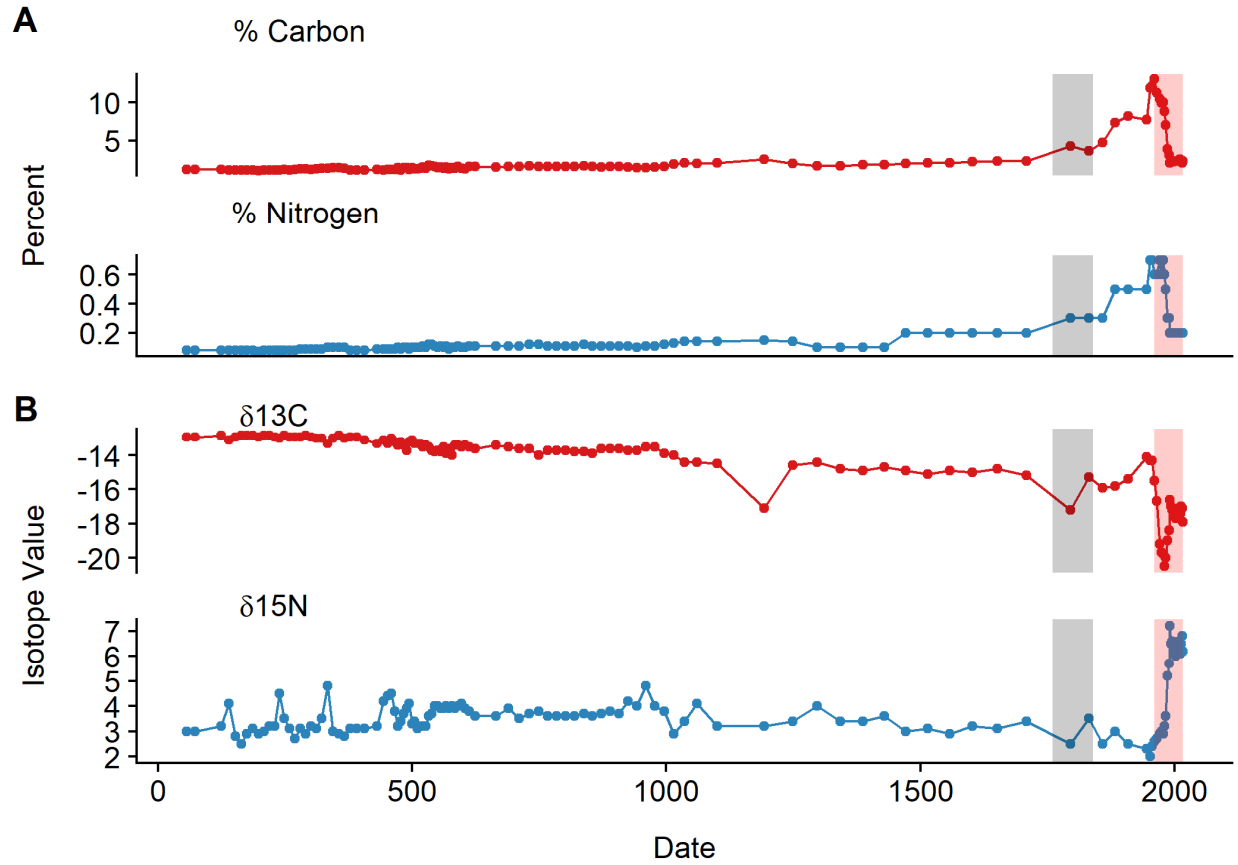


Figure 9. **(A)** Percent of carbon (C) and nitrogen (N) and **(B)**  $\delta^{13}\text{C}$  and  $\delta^{15}\text{N}$  in the Upper Wetland core (UC11) from 0 AD to present day. Gray box indicates the Industrial Revolution (~1760-1840) and the red box indicates the deforestation in the Mau Forest (~1964-Present) (Baldyga et al., 2008).

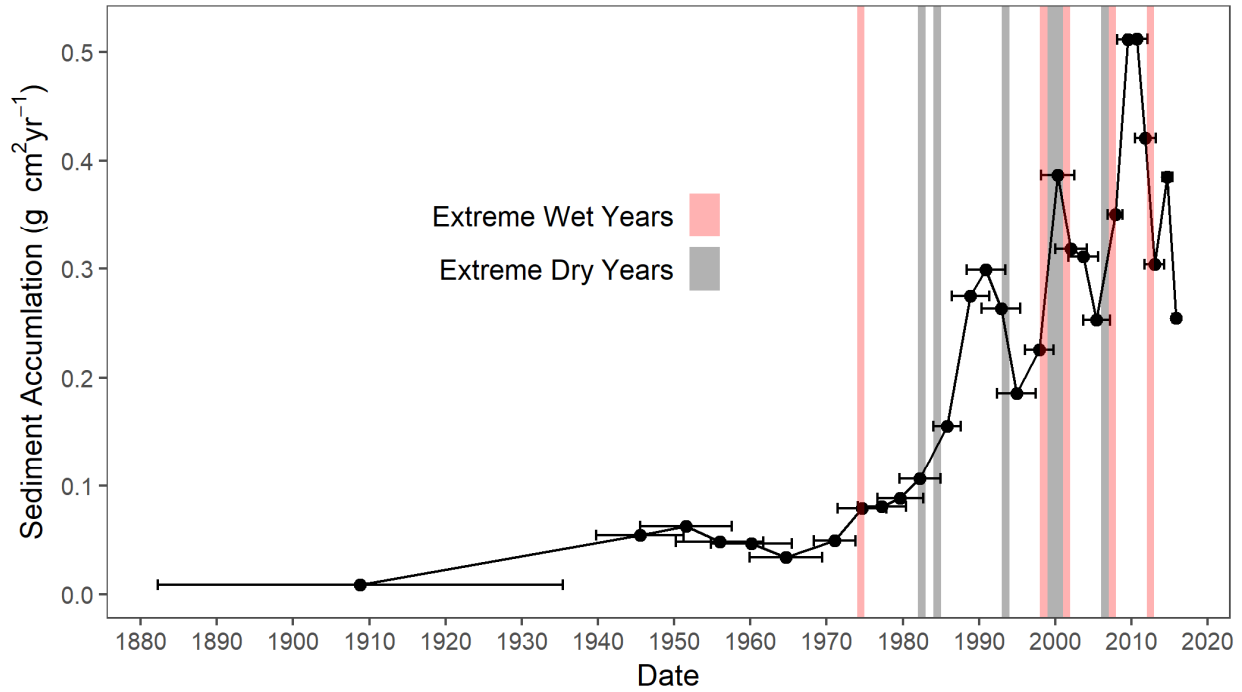


Figure 10. Sediment accumulation for the Upper Wetland core from 1900 until 2015. Horizontal error bars indicate Bayesian modelled uncertainty from the age-depth model. Years experiencing extreme rainfall with a greater than a 10-year return interval for wet years (red) and dry years (gray) are indicated as shaded bars (Bartzke et al., 2018). Yearly rainfall data only available since 1965.

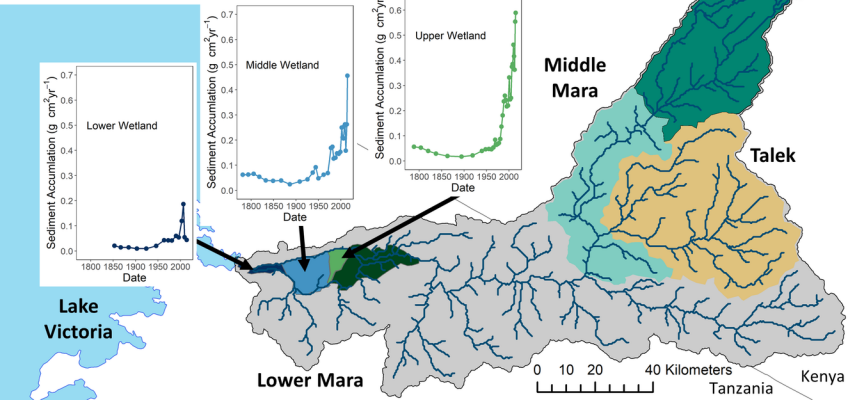
## Tables

Table 1. Radiocarbon chronology of the Seasonal Wetland core set (UC7, RC9, RC10, RC11, and RC12) and the Upper Wetland core set (UC11, RC21, RC23) from the Mara Wetland.

Laboratory code	Material	Core Set	Core	Depth (cm)	Thickness (cm)	14C age [yr BP]	Calibrated age [cal yr BP, $\pm 1 \sigma$ ] <sup>1</sup>
CAMS# 173870	TOC of bulk sediment	Seasonal Wetland	RC9	48	1	300 $\pm$ 30	362 $\pm$ 106
CAMS# 173869	TOC of bulk sediment	Seasonal Wetland	RC10	88	1	Modern	Modern
CAMS# 173871	TOC of bulk sediment	Seasonal Wetland	RC11	128	1	285 $\pm$ 30	336 $\pm$ 119
CAMS# 174604	TOC of bulk sediment	Seasonal Wetland	RC12	159	1	Modern	Modern
CAMS# 172566	TOC of bulk sediment	Seasonal Wetland	RC12	189	1	2625 $\pm$ 50	2691 $\pm$ 147
CAMS# 174605	TOC of bulk sediment	Upper Wetland	UC11	44	1	995 $\pm$ 45	898 $\pm$ 97
CAMS# 174606	TOC of bulk sediment	Upper Wetland	RC21	67	1	1445 $\pm$ 35	1393 $\pm$ 74
CAMS# 174607	TOC of bulk sediment	Upper Wetland	RC23	97	1	1610 $\pm$ 40	1518 $\pm$ 102
CAMS# 172565	TOC of bulk sediment	Upper Wetland	RC23	124	1	1910 $\pm$ 45	1839 $\pm$ 119

<sup>1</sup> Using the IntCal13 calibration curve (Reimer et al., 2013) in *Bchron* in R (Parnell, 2016).

The Mara Wetland buffers Lake Victoria:  
Higher rates of sediment accumulation in  
upstream portions of wetland



Rapid and increasing sediment  
accumulation in the Mara  
Wetland from major portions of  
the basin since the 1960s

